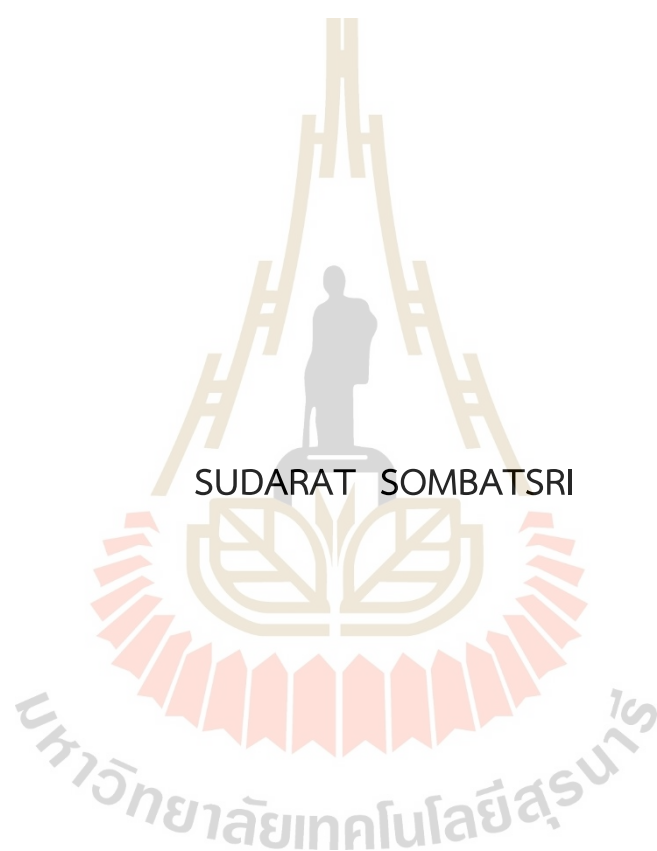


PYRANINE IMMOBILIZED ON AMINOPROPYL-MODIFIED
MESOPOROUS SILICA FILM FOR PARAQUAT DETECTION



A Thesis Submitted in Partial Fulfillment of the Requirements for the
Degree of Doctor of Philosophy in Chemistry
Suranaree University of Technology
Academic Year 2022

ไพรรานินตริงบนฟิล์มซิลิกาเมโซพอร์ที่ดัดแปรด้วยอะมิโนโพรพิลเพื่อการ
ตรวจวัดพาราควอต



นางสาวสุดารัตน์ สมบัติศรี

วิทยานิพนธ์นี้เป็นส่วนหนึ่งของการศึกษาตามหลักสูตรปริญญาวิทยาศาสตรดุษฎีบัณฑิต
สาขาวิชาเคมี
มหาวิทยาลัยเทคโนโลยีสุรนารี
ปีการศึกษา 2565

PYRANINE IMMOBILIZED ON AMINOPROPYL-MODIFIED MESOPOROUS
SILICA FILM FOR PARAQUAT DETECTION

Suranaree University of Technology has approved this thesis submitted in
partial fulfillment of the requirements for the Degree of Doctor of Philosophy.

Thesis Examining Committee



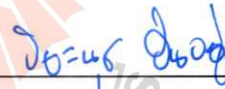
(Assoc. Prof. Dr. Anyanee Kamkaew)
Chairperson



(Assoc. Prof. Dr. Sanchai Prayoonpokarach)
Member (Thesis advisor)



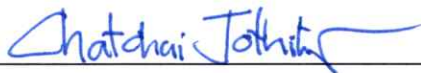
(Prof. Dr. Jatuporn Wittayakun)
Member



(Dr. Piyanut Pinyou)
Member



(Asst. Prof. Dr. Sirinuch Loiha)
Member



(Assoc. Prof. Dr. Chatchai Jothityangkoon)
Vice Rector for Academic Affairs
and Quality Assurance



(Prof. Dr. Santi Maensiri)
Dean of Institute of Science

สุดารัตน์ สมบัติศรี : ไพราซีนตรึงบนฟิล์มซิลิกาเมโซพอร์ที่ดัดแปรด้วยอะมิโนโพรพิลเพื่อ
การตรวจวัดพาราควอต (PYRANINE IMMOBILIZED ON AMINOPROPYL-MODIFIED
MESOPOROUS SILICA FILM FOR PARAQUAT DETECTION) อาจารย์ที่ปรึกษา :
รองศาสตราจารย์ ดร.สัญญาชัย ประยูรโกศราช, 65 หน้า

คำสำคัญ: ฟิล์มซิลิกาเมโซพอร์/ พาราควอต/ ไพราซีน/ ฟลูออเรสเซนซ์

วิธีการตรวจวัดพาราควอตในสารละลายในน้ำพัฒนาขึ้นมาโดยใช้เซ็นเซอร์เคมีเชิงแสงที่สร้าง
จากการตรึงไพราซีนบนฟิล์มซิลิกาเมโซพอร์ที่ดัดแปรด้วยหมู่อะมิโนโพรพิล ฟิล์มซิลิกาเมโซพอร์
สังเคราะห์เคลือบไว้บนแผ่นแก้วที่มีทินออกไซด์เจือด้วยฟลูออรีนโดยวิธีการประกอบตัวเองร่วมกับการ
ช่วยทางเคมีไฟฟ้า ฟิล์มที่สังเคราะห์ได้นำไปวิเคราะห์ลักษณะด้วยหลายเทคนิคได้แก่ เทคนิคไซ
คลิกโวลแทมเมตรี เทคนิคจุลทรรศน์อิเล็กตรอนแบบส่องกราด เทคนิคจุลทรรศน์อิเล็กตรอนแบบส่อง
ผ่าน เทคนิคฟูเรียร์ทรานส์ฟอร์มอินฟราเรดสเปกโทรสโกปี และเทคนิคฟลูออเรสเซนซ์สเปกโทรสโกปี

ฟิล์มซิลิกาเมโซพอร์แบบชั้นเดียวความหนา ~170 นาโนเมตรและช่องว่างตัวตั้งฉากกับพื้นผิว
แก้วสังเคราะห์ได้จากการใช้เตตระเอทิลออร์โทซิลิเกตเป็นแหล่งให้ซิลิกา ฟิล์มมีความโปร่งแสงและมี
ความเสถียรทางกายภาพและทางเคมีในสารละลายในน้ำ ฟิล์มซิลิกาเมโซพอร์นี้จะดัดแปรด้วย 3-อะมิ
โนโพรพิล ไตรเอทอกซีไซเลนก่อนนำไปตรึงด้วยไพราซีน ฟิล์มที่เหมาะสมที่สุดสำหรับนำไปใช้นั้นดัดแปร
ด้วยสารละลาย 3-อะมิโนโพรพิล ไตรเอทอกซีไซเลนเข้มข้นร้อยละ 3 โดยปริมาตร และไพราซีนที่ตรึง
ได้บนแผ่นฟิล์มมีปริมาณ 1.75×10^{-4} มิลลิโมล

ฟิล์มที่ตรึงด้วยไพราซีนเกิดแสงฟลูออเรสเซนซ์ที่ 506 นาโนเมตร เมื่อกระตุ้นที่ 450 นาโน
เมตร และสัญญาณฟลูออเรสเซนซ์ลดลงเมื่อมีพาราควอตอยู่ด้วย วิธีการที่พัฒนาขึ้นแสดงการ
ตอบสนองเชิงเส้นต่อพาราควอตในช่วงความเข้มข้น 1 ถึง 10 ppm ในสภาวะที่ปรับให้เหมาะสม โดย
มีขีดจำกัดการตรวจวัดที่ 0.80 ppm วิธีการนี้นำไปประยุกต์ใช้หาปริมาณพาราควอตในตัวอย่าง
เปลือกอ้อยและน้ำประปาได้สำเร็จ

สาขาวิชาเคมี

ปีการศึกษา 2565

ลายมือชื่อนักศึกษา สุดารัตน์ สมบัติศรี

ลายมือชื่ออาจารย์ที่ปรึกษา ดร.สัญญาชัย

ACKNOWLEDGEMENTS

I would like to express my gratitude to all the individuals who have assisted me in completing my Ph.D. journey.

First and foremost, I would like to express my profound and sincere appreciation to Assoc. Prof. Dr. Sanchai Prayoonpokarach for his unwavering support, immense expertise, encouragement, and guidance from the beginning of this research to its culmination. I cannot imagine having had a better advisor and mentor for my research.

Furthermore, I would like to extend my gratitude to the thesis committee and Rajamangala University of Technology Isan for providing me with a wonderful opportunity to conduct this exciting research.

I would also like to express my appreciation to all the lecturers in the School of Chemistry, Suranaree University of Technology, for their good-natured attitudes and valuable advice.

To my dear friends in the research group (Nickky, Jack, Bee, Mai, Fluck and Pae), thank you for supporting my research activities.

Lastly, I want to express my deepest gratitude to my family for their love, understanding, encouragement, and unwavering support throughout my education.

Sudarat Sombatsri

CONTENTS

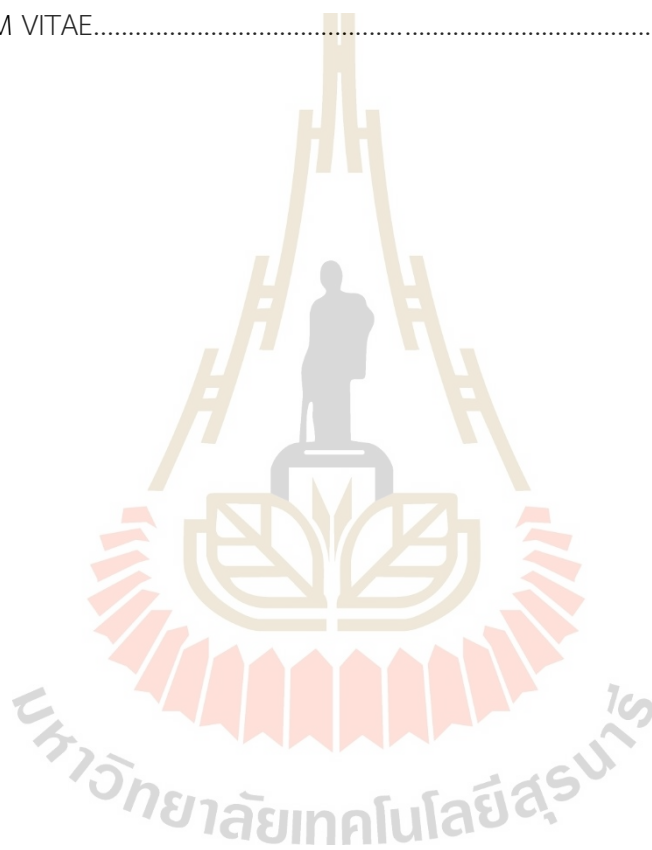
	Page
ABSTRACT IN THAI.....	I
ABSTRACT IN ENGLISH.....	II
ACKNOWLEDGEMENTS.....	III
CONTENTS.....	IV
LIST OF TABLES.....	VII
LIST OF FIGURES.....	VIII
CHAPTER	
I INTRODUCTION.....	1
1.1 Significance of the study.....	1
1.2 Chemical sensors.....	2
1.3 Research objectives.....	4
II LITERATURE REVIEW.....	5
2.1 Background of chemical sensors for paraquat.....	5
2.2 Sensing reagents for paraquat.....	6
2.3 Supporting matrix.....	8
III EXPERIMENTAL.....	13
3.1 Chemicals.....	13
3.2 Synthesis of mesoporous silica films.....	14
3.2.1 Stöber solution growth method.....	14
3.2.2 Electrochemically assisted self-assembly method.....	15
3.3 Modification of MSFs with 3-aminopropytriethoxysilane.....	16
3.4 Immobilization of pyranine on NH ₂ -MSFs.....	16
3.5 Characterization of MSFs, NH ₂ -MSFs and pyranine-immobilized MSFs....	16
3.6 Response of sensing film to paraquat.....	17
3.7 Calibration study for paraquat.....	17
3.8 Regeneration of sensing film.....	17

CONTENTS (Continued)

	Page
3.9 Reproducibility and repeatability.....	18
3.10 Interference study.....	18
3.11 Analysis of real samples.....	18
IV RESULTS AND DISCUSSION.....	20
4.1 Characterization of MSFs from the Stöber solution growth method.....	21
4.2 Characterization of MSFs synthesis via the EASA method.....	24
4.2.1 Characterization of MSFs obtained from TEOS as silica source.....	24
4.2.2 Characterization of MSFs obtained from sodium silicate as silica source.....	30
4.3 Characterization of the multilayer films obtained from using tetraethyl orthosilicate as silica source.....	34
4.4 Characterization of mesoporous silica films modified with 3-aminopropyltriethoxysilane.....	37
4.4.1 Functional groups analysis of NH ₂ -MSF by FTIR.....	37
4.4.2 Permeability of NH ₂ -MSF by cyclic voltammetry.....	38
4.5 Immobilization of pyranine on MSFs.....	40
4.6 Optimization of sensing films.....	43
4.6.1 Effect of APTES concentration on the immobilization of pyranine	43
4.6.2 Time for pyranine immobilization.....	44
4.6.3 Effect of pH on the fluorescence of pyranine-immobilized film.....	44
4.6.4 Reproducibility of sensing film fabrication.....	45
4.7 Performance characteristics of sensing films.....	47
4.7.1 Response of sensing film to paraquat.....	47
4.7.2 Calibration graph for paraquat.....	49
4.7.3 Reproducibility and regeneration.....	50
4.7.4 Interference study.....	52

CONTENTS (Continued)

	Page
4.8 Real sample analysis.....	53
V CONCLUSIONS.....	55
REFERENCES.....	57
APPENDIX.....	63
CURRICULUM VITAE.....	65



LIST OF TABLES

Table		Page
2.1	Synthesis conditions and important characters of MSFs obtained from three synthesis methods.....	11
3.1	Chemicals used in this research.....	13
4.1	Interference study at 1:5 molar ratio of PQ to interference species	53
4.2	Determination of PQ in tap water and sugarcane peel samples.....	53
4.3	Different methods used for detection of PQ.....	54



LIST OF FIGURES

Figure	Page
1.1 A chemical structure of PQ.....	2
1.2 A simplified diagram of the main components of a chemical sensor.....	3
4.1 (a) A picture of the film synthesized by the Stöber solution growth method using TEOS as a silica source and (b) SEM image of the film.....	21
4.2 Cyclic voltammograms of bare FTO electrode and MSF-ST/FTO electrode before and after surfactant removal recorded in a solution containing 0.5 mM $\text{Ru}(\text{NH}_3)_6^{3+}$ and 0.1 M NaNO_3 . The scan rate was 0.1 Vs^{-1} . The electrode size is $0.9 \times 0.9 \text{ cm}$	22
4.3 Cyclic voltammograms of the FTO electrode before and after the synthesis using sodium silicate as a silica source. The same conditions for voltammetric measurements as in Figure 4.2 were used.....	23
4.4 Photographic image of MSFs/FTO with various deposition time after surfactant removal.....	24
4.5 Cyclic voltammograms of MSF-EASA-TEOS/FTO electrodes recorded in 0.1 M NaNO_3 solutions containing (a) 5.0 mM $\text{Ru}(\text{NH}_3)_6^{3+}$ and (b) 5.0 mM $\text{Fe}(\text{CN})_6^{3-}$. The scan rate was 0.1 Vs^{-1}	25
4.6 FTIR spectra of MSF-EASA-TEOS/FTO glass, before/after surfactant removal and on bare FTO electrode.....	26
4.7 SEM images of MSFs/FTO from different deposition time a) top view and b) cross-section.....	28
4.8 MSFs with various deposition time; CV of 5 mM $\text{Ru}(\text{NH}_3)_6^{3+}$ redox probe in 0.1 M NaNO_3 solution on MSFs-T/FTO after surfactant removal and on bare FTO electrode; Scan rate 0.1 Vs^{-1} , Surface area of electrode is $0.9 \times 0.9 \text{ cm}$	29
4.9 TEM images of MSFs after peeling off from FTO substrate	29

LIST OF FIGURES (Continued)

Figure	Page
4.10 (a) Cyclic voltammogram of 5 mM $\text{Ru}(\text{NH}_3)_6^{3+}$ redox probe in 0.1 M NaNO_3 solution on film/FTO before surfactant removal with different Na_2SiO_3 initial content (b) XRD pattern of the precipitation of silica in hydrolyzed sol.....	31
4.11 Cyclic voltammograms of the electrodes synthesized with different hydrolysis times without surfactant removal recorded in a solution containing 5 mM $\text{Ru}(\text{NH}_3)_6^{3+}$ and 0.1 M NaNO_3	32
4.12 Cyclic voltammograms of the electrodes synthesized with different deposition times without surfactant removal recorded in a solution containing 5 mM $\text{Ru}(\text{NH}_3)_6^{3+}$ and 0.1 M NaNO_3	33
4.13 SEM image of a) bare FTO b) thin film on FTO.....	34
4.14 SEM images of mMSF-TEOS /FTO. xL indicates the number of deposition layers where x = 1, 2, 3 or 4.....	35
4.15 Cyclic voltammograms of 5 mM $\text{Ru}(\text{NH}_3)_6^{3+}$ redox probe in 0.1 M NaNO_3 solution on mMSF-TEOS/FTO, before (a) and after (b) surfactant removal; scan rate: 0.1 mVs^{-1} , electrode area: $0.9 \times 0.9 \text{ cm}^2$	36
4.16 FTIR spectra of NH_2 -MSF from various concentrations of APTES used in the modification.....	38
4.17 Cyclic voltammograms of a) 5 mM $\text{Ru}(\text{NH}_3)_6^{3+}$ and b) 5 mM $\text{Fe}(\text{CN})_6^{3-}$ redox probe in 0.1 M NaNO_3 solution on modified MSFs with various concentrations of APTES, on MSF and on bare FTO electrode; Scan rate 0.1 Vs^{-1} , the size of the electrode is $0.9 \times 0.9 \text{ cm}^2$	39
4.18 Cyclic voltammograms of 5 mM $\text{Fe}(\text{CN})_6^{3-}$ redox probe in 0.1 M NaNO_3 solution on NH_2 -multilayer MSF; Scan rate 0.1 mVs^{-1} , the size of the electrode is $0.9 \times 0.9 \text{ cm}^2$	40
4.19 Fluorescence spectra of pyranine immobilized on MSF and a photograph of the film	41

LIST OF FIGURES (Continued)

Figure	Page
4.20 a) Fluorescence spectra of monolayer MSF and multilayered-MSFs b) a photograph of pyranine immobilized films.....	42
4.21 Fluorescence spectra of sensing films modified with various APTES concentrations in buffer pH 6.0.....	43
4.22 Fluorescence spectra of sensing films at various immobilization times.....	44
4.23 Fluorescence spectra of sensing films in buffer at different pH.....	45
4.24 Fluorescence signals of sensing films at 506 nm, (a) films from the same batch, (b) films from different batches.....	46
4.25 a) Fluorescence emission spectra of a sensing film before and after immersing in 10.0 ppm (3.89×10^{-5} M) paraquat solution, b) Time profiles of response signals at 506 nm of the sensing films with paraquat at different concentrations.....	48
4.26 Time profiles of response signals of the sensing films coated with Nafion.....	49
4.27 Calibration curve for paraquat. An inset shows a linear relationship for PQ concentration range of 1-10 ppm.....	50
4.28 The recycling process for one sensing film.....	51
4.29 Regeneration of the sensing film.....	52

CHAPTER I

INTRODUCTION

1.1 Significance of the study

Pesticides are chemical substances used in agricultural, industrial, and residential settings to control or eliminate pests such as insects, weeds, fungi, and rodents. They contribute significantly to food security and agricultural productivity by protecting crops from pests and diseases. Pesticides can be classified into different types, including insecticides, herbicides, fungicides, and rodenticides depending on their target organisms. Despite their benefits, pesticides can also have harmful effects on human health and the environment.

1,1'-Dimethyl-4,4'-dipyridinium chloride or paraquat (PQ) is one of the pesticides typically used to eliminate broadleaf weeds in agricultural and non-agricultural areas due to its high efficiency and relatively low cost. The chemical structure of PQ is shown in Figure 1. PQ can cause various human health problems. The toxicity of PQ is associated with the reduction of a divalent cation (PQ^{2+}) to a free radical ($PQ^{+•}$), which generates a superoxide radical and singlet oxygen upon reacting with oxygen (Bus, 1976). These reactive radicals could damage cell membranes, proteins, and DNA (Peter, 1992). Humans are likely to be exposed to PQ through food crops and drinking water. Depending on the concentration, ingestion of PQ could cause liver and kidney failure and lung scarring. The lethal dose in humans is approximately 35 mg/kg (Tsai, 2013). The Thai Agriculture Standard (TAS 9002-2008) recommends a maximum residue limit (MRL) of 0.05 mg/kg of PQ in fruits and vegetables, which is similar to the value recommended by the Food and Agriculture Organization of the United Nations (FAO) and the World Health Organization (WHO). The United States Environmental Protection Agency (US EPA) has set a regulated maximum contaminant level of 3 $\mu\text{g/L}$ for PQ in drinking water. Therefore, regularly monitoring and determining the concentration of PQ is crucial. Various analytical methods have been developed to accurately detect

PQ residues, including chromatography, immunoassays, and biosensors, which provide reliable and sensitive detection of PQ in various matrices.

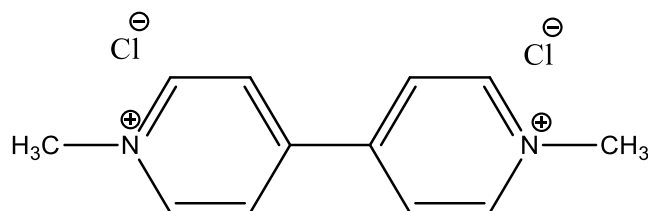


Figure 1.1 A chemical structure of PQ.

Chromatographic methods, such as gas chromatography-mass spectrometry (GC-MS) (Gao et al., 2015) and high-performance liquid chromatography (HPLC) (Sha et al., 2018), are commonly used for the detection of PQ. These techniques offer good selectivity, sensitivity, and the ability to detect multiple analytes. However, they require sophisticated equipment, tedious sample preparation, skilled operators, and lengthy analysis times. In some cases, a specific pesticide needs to be identified, making a rapid, straightforward, and cost-effective method desirable. Nevertheless, the method must still be able to detect PQ at the relevant concentrations. An alternative analytical method for PQ based on chemical sensors is of interest in this work.

1.2 Chemical sensors

A chemical sensor can be defined as a device that transforms chemical information from the interaction between an analyte and the device into analytical signals. The sensor is designed for detecting and measuring the presence of specific analytes in a given environment. Detection mechanisms of chemical sensors rely on the interaction between the target analyte and the sensing element, which can be based on different principles, including chemical reactions or physical changes in the sensing element. Chemical sensors have a wide range of applications, including environmental monitoring, medical diagnostics, food safety, and industrial process control. Generally, a chemical sensor typically consists of two major components: a

receptor part, which serves as an analyte recognition system, and a transducer. Figure 1.2 illustrates a simplified diagram of a chemical sensor device. Chemical sensors can be classified according to the transducer types as optical, electrochemical, mass-sensitive, and heat-sensitive sensors (Baldini et al., 2006).

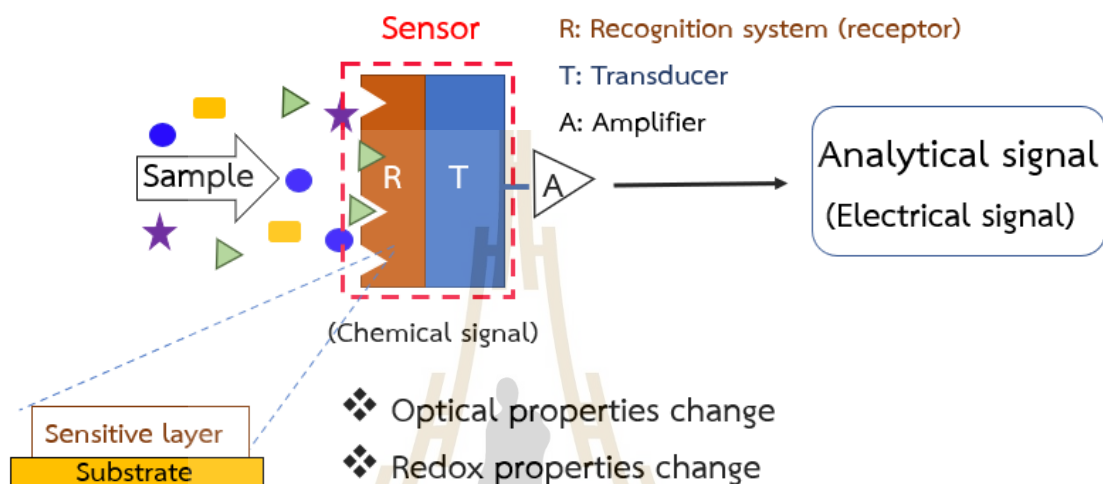


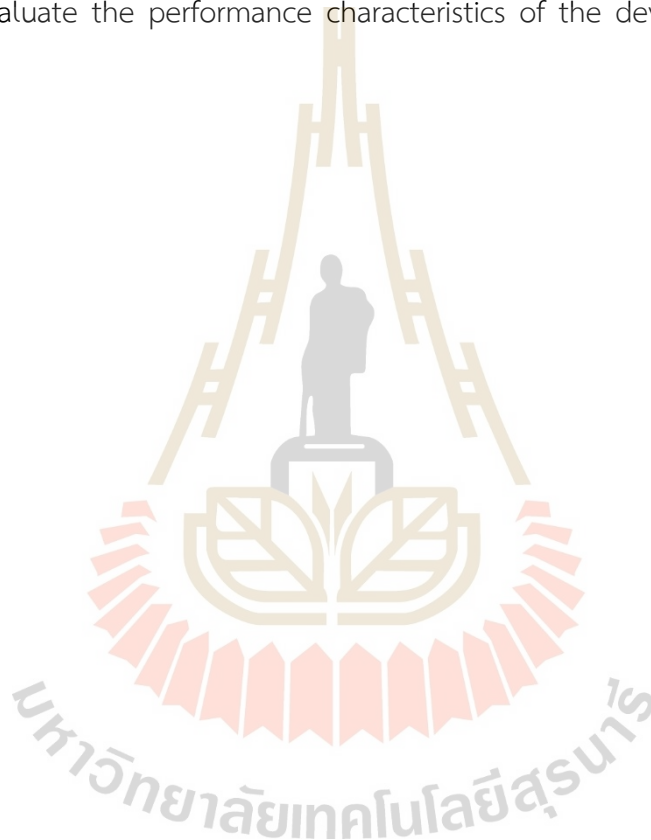
Figure 1.2 A simplified diagram of the main components of a chemical sensor.

This research aims to develop an optical chemical sensor for PQ, focusing mainly on developing the receptor part to respond selectively to PQ. The receptor component was designed to consist of a sensing reagent and a supporting matrix. The supporting matrix is responsible for immobilizing the sensing reagent and should possess certain characteristics, including homogeneity, compatibility with the sensing reagent, transparency with low intrinsic absorbance or fluorescence, and long-term physical and chemical stability. Mesoporous silica films (MSFs) were used as a supporting matrix in this work and synthesized on fluorine-doped tin oxide (FTO) coated glass slides using an electrochemically assisted self-assembly (EASA) method (Walcarius et al., 2007) and Stöber solution growth method (Teng et al., 2012).

1.3 Research objectives

The objectives of this thesis are as follows:

1. To develop a method for determining PQ using 8-hydroxypyrene-1,3,6-trisulfonic acid trisodium salt or pyranine immobilized on a modified MSF supported on FTO.
2. To synthesize MSFs on FTO via the EASA method and Stöber solution growth method and study modified MSFs capability to support pyranine.
3. To evaluate the performance characteristics of the developed materials for detecting PQ.



CHAPTER II

LITERATURE REVIEW

The literature review is divided into two parts. The first part covers the background of chemical sensors used for detecting paraquat and the second part focuses on the major components that make up a chemical sensor.

2.1 Background of chemical sensors for paraquat

Paraquat (PQ) is a widely used herbicide that poses a significant health risk upon ingestion or skin/eye contact due to its known toxicity. Exposure to PQ for humans is likely through food crops and drinking water residues. Therefore, analytical methods providing reliable results in determining PQ concentration in such samples are crucial. Currently, chromatographic techniques such as gas chromatography-mass spectrometry (GC-MS) (Gao et al., 2015) and high-performance liquid chromatography (HPLC) (Sha et al., 2018) are commonly used for the determination of PQ in various samples. However, these methods require sample treatment, expensive and sophisticated instruments, and skilled operators. Alternative methods for PQ are therefore being developed to meet specific needs. Chemical sensors are alternative to traditional methods due to their advantages, such as equipment simplicity, cost-effectiveness, analysis speed, sensitivity, and selectivity. They can detect PQ at environmentally relevant levels and provide real-time or near-real-time results. Consequently, there is a growing interest in developing chemical sensors for PQ detection in various samples, including fruits, vegetables, and water.

Electrochemical and optical sensors have shown promise in detecting PQ in recent years. Chemically modified electrodes have been extensively researched for this purpose. Various chemical materials, including mesoporous silica films on a glassy carbon electrode (GCE) (Nasir et al., 2018), phospholipid layers with asolectin on GCE (Tomková et al., 2018), β -cyclodextrin/smectite clay composites on GCE (Tcheumi et

al., 2019), and gold nanocrosses-chitosan on GCE (Shan et al., 2019), have been used for electrode modification. Modification of the electrode surface usually leads to increased selectivity and sensitivity of the analysis. However, electrochemical methods have some disadvantages, such as the requirement of electrical contact for a wire conductor and electrode materials, slow electron transfer rate after electrode modification, and poisoning of the electrode surface by species in a solution.

Optical chemical sensors can provide an alternative method for detecting PQ. They offer a simple and rapid approach based on measuring fluorescence, absorbance, Raman, or surface plasmon resonance (SPR) signals. Typically, an optical chemical sensor consists of an analyte recognition unit and a transducer. The recognition element, such as analyte complexing agents, enzymes, and indicator dyes, is usually immobilized in a supporting matrix. Polymers and porous materials are common supports for the recognition element.

2.2 Sensing reagents for paraquat

The development of chemical sensors for PQ relies on selecting a suitable sensing reagent that can interact specifically with the target molecule and a signal transduction element that can convert the binding event into a measurable signal. The recognition element, a crucial component of the sensors, can be chosen from a wide range of materials, including antibodies, aptamers, molecularly imprinted polymers (MIPs), or other receptor molecules, depending on the desired level of selectivity and sensitivity. The transduction element can be based on various principles, such as electrochemical, optical, or mass-based, to meet the application's specific requirements. In addition, factors such as selectivity, sensitivity, speed, and cost-effectiveness are taken into account.

Maya et al. (2011) previously employed an ascorbic acid-based reagent in a novel multisyringe flow injection analysis to detect a limit of detection of 0.003 μM . Meanwhile, Siangproh et al. (2017) utilized citrate-stabilized Ag nanoparticles as a colorimetric probe for PQ detection. They observed that PQ induced the aggregation of negatively charged silver nanoparticles via coulombic attraction, resulting in a color change that was directly proportional to the concentration of PQ. This method could

detect PQ in the concentration range of 0.2 to 7.8 μM , with a detection limit of 0.074 μM . Furthermore, other research groups have used colorimetry techniques for PQ analysis, such as utilizing sodium 3-mercaptopropanesulfonate modified Au nanoparticles (Zhang et al., 2020) and imidacloprid stabilized Ag nanoparticles (Ali et al., 2022) where the limit of detection are 0.004 and 6.3 μM , respectively.

Fluorescence is a commonly utilized technique in laboratories due to its sensitivity and simplicity in detecting a range of analytes. To detect PQ, Tu et al. (2015) developed fluorescence "off-on" method for detecting PQ based on the surfactant-controlled aggregate-deaggregate mechanism of squaraines and sodium dodecyl sulfate (SDS). This system showed high selectivity for PQ, with a limit of detection of 0.372 μM . Du et al. (2019) developed a novel fluorescence "on-off-on" method for the detection of Hg^{2+} and paraquat using nitrogen-doped graphene quantum dots (N-GQDs) and N-GQDs/ Hg^{2+} system, respectively. The N-GQDs solution fluorescence was quenched in the presence of Hg^{2+} ions (turn-off), and the quenched N-GQDs/ Hg^{2+} system was recovered after the addition of paraquat (turn-on). The method demonstrated high selectivity and sensitivity, with the detection limits for paraquat was 0.074 μM . In addition, some researches have focused on the fluorescent quenching method. Duran et al. (2011) found that CdSe/ZnS quantum dots could be employed to detect PQ in water samples. They synthesized the catalyst and made it water-soluble through the use of hydrophilic thiol ligands. They then utilized the catalyst in fluorescence methods to detect PQ and observed that it was effective in detecting the target analyte in a detection limit of 0.012 μM . Yao et al. (2013) utilizes the significant quenching of the fluorescence intensity of a cucurbit[7]uril-coptisine fluorescent probe due to the supramolecular inclusion interaction with PQ. The method showed excellent sensitivity, with detection in the range of 0.1 nM to 0.12 μM , and the detection limit was determined to be 3.35 nM. This novel method provides a highly sensitive and selective approach to detect PQ in various environmental samples.

Recently, Zhao et al. (2018) studied the determination of PQ using 8-hydroxypyranin-1,3,6-trisulfonate or pyranine as a reagent. They found that PQ induced the quenching of pyranine fluorescence signal in aqueous solutions. Although this method showed good sensitivity and selectivity to PQ, the pyranine solution was used

and disposed of after the reaction. In addition to its use as a reagent for PQ, pyranine was also utilized in the detection of intracellular pH (Han and Burgess, 2010), CO₂ gas (Dansby-Sparks et al., 2010), and Cu⁺ in vitro (Saha et al., 2014).

Several solid supports have been utilized to immobilize pyranine, such as ethyl cellulose (Hakonen and Hulth, 2008), poly(dimethyl siloxane) with poly(2-hydroxyethyl acrylate) (Ulrich et al., 2019), and organo-silica sol-gel membranes (Nivens et al., 2002). However, these materials were mainly used as optical pH sensors. There are no reports of pyranine immobilized on porous solid supports as sensors for PQ. Porous materials are preferred for immobilization because of their high surface area, which allows for a large amount of reagent to be immobilized and aids the accessibility of the analyte to the sensing sites. Therefore, this study focuses on immobilizing pyranine on a suitable porous support. Immobilizing the reagent on the support could enhance sensitivity and selectivity, permit reagent reusability, and reduce waste generation.

2.3 Supporting matrix

Supporting matrices provide a surface for immobilizing the sensing element or indicator. Selecting a supporting matrix is critical in determining the optical sensor's sensitivity, selectivity, and stability. The ideal supporting matrix should have high porosity, good permeability for the analyte, and minimal interference with the sensing element. Furthermore, it should be chemically inert and compatible with the analyte and the sensing environment. Zeolites, silica gel, polymers, glass, and quartz are examples of matrices used in optical sensors.

Porous materials are used in various applications such as catalysis, chemical separation, adsorption, and sensors due to high surface area, narrow pore size distribution, capability for framework substitution with various metal oxides, and simple functionalization strategies with organic molecules. According to the definition of the International Union of Pure and Applied Chemistry (IUPAC), porous materials can be classified into three types based on pore size, including microporous (pore size <2 nm), mesoporous (pore size: 2-50 nm), and macroporous (pore size >50 nm) materials.

Mesoporous materials can be synthesized from a variety of precursors such as silica, transition metal oxides, carbon, hybrid materials, or organic polymers, and can

have various morphologies. This research used mesoporous silica films (MSFs) to immobilize pyranine. Mesoporous silica possesses various pore structures and orientations, high surface area, and high thermal stability. Silanol groups on the silica surface can be functionalized with organic groups (Innocenzi and Malfatti, 2013). Several methods exist for synthesizing mesoporous silica using cationic surfactants as a structure-directing agent. Mesoporous structures occur via hydrolysis and condensation of silica precursors around micelle templates. The templates can be removed by calcination or solvent extraction. Tetraethoxysilane (TEOS) and sodium silicate are commonly used as silica precursors in the synthesis.

Mesoporous silica films (MSFs) have gained interest in sensing applications due to their properties. Various structures of MSFs can be synthesized by controlling the synthesis conditions. The favorable properties of MSFs for sensors include their continuous and homogeneous thin film and their uniform pore structure and orientation.

There are various methods for preparing MSFs. The evaporation-induced self-assembly (EISA) method is one of the methods used for generating thin silica films. In this technique, a mixture of silica precursor and surfactant in a water-alcohol solution is applied to a solid support. As the solution evaporates, a film forms on the support surface. The solution can be deposited using dip-coating, spray-coating, or spin-coating techniques. This method can produce a range of pore structures, including 2D or 3D structures and worm-like structures (Grosso et al., 2004; Kanno et al., 2012). However, MSFs obtained using the EISA method have limited sensing applications because their structures are randomly oriented on the substrate surface, which may hinder mass transport and accessibility to active sites. MSFs with pore channels oriented perpendicular to the support surface are needed to mitigate the disadvantages of those from the EISA method.

The Stöber solution growth method and the electrochemically assisted self-assembly (EASA) method are used to produce MSFs with mesoporous channels vertically oriented to the support surface. The Stöber solution growth method (Stöber et al., 1968) is applied for synthesizing spherical silica particles by hydrolyzing a silica precursor and condensing silicic acid in an alcoholic solution with ammonia as a

catalyst. Using this method, Teng et al. (2012) successfully synthesized MSFs with mesoporous channels aligned perpendicular to glass and indium tin oxide-coated glass. They immersed the glass substrate in a Stöber solution containing TEOS, hexadecyltrimethylammonium bromide (CTAB), ammonia, and ethanol under hydrothermal conditions at 60 °C for various times. CTAB cations adsorb and form spherical micelle assemblies on the negatively charged substrate, and TEOS slowly hydrolyzes in the basic solution to form negatively charged silicate around the micelles. Ammonia catalyzes the polycondensation of silicate species, leading to the growth of mesoporous channels vertically aligned to the substrate surface. The surfactant removal is done by extraction or calcination. The mesoporous channels are highly oriented and perpendicular to the substrate surface, with excellent mechanical and chemical stability. However, this method takes a long time, ranging from 3 to 72 hours.

Walcarius et al. (2007) first reported the EASA method for preparing mesoporous silica films with vertically aligned pore channels. This method involves electrodeposition, wherein a suitable cathodic potential is applied to an electrode submerged in a hydrolyzed sol solution containing TEOS and a surfactant such as CTAB in a water/ethanol acid solution. The time for the potential application is <60 s. The applied potential generates hydroxide ions that catalyze polycondensation of the silicate species, leading to the formation of templated silica mesopore channels growing perpendicularly on the electrode surfaces (Herzog et al., 2013).

The thickness of vertically aligned MSFs can be controlled in the 25-150 nm range by varying the applied potential and deposition time (Goux et al., 2009). However, using too high an applied potential or too long deposition time results in silica aggregates on the surface of MSFs (Ding and Su, 2015). Multilayer and vertically aligned films without silica aggregates can be synthesized to obtain a film thickness of approximately 400 nm by consecutive potentiostatic EASA steps (Giordano et al., 2017). The EASA method is faster, cheaper, and easier to operate than the Stöber-solution growth method. However, this method requires a conductive substrate. The synthesis conditions and characteristics of MSFs synthesized by the three methods are summarized in Table 2.1.

Table 2.1 Synthesis conditions and important characters of MSFs obtained from three synthesis methods.

	EISA method	EASA method	Stöber-solution growth method
Conditions	<ul style="list-style-type: none"> • a sol-gel mixture deposition on a solid substrate by dip-, spin-, or spray-coating • time for film formation, 2-40 min 	<ul style="list-style-type: none"> • requires a conductive substrate and a potentiostat • 5-30 s for film deposition 	<ul style="list-style-type: none"> • a solid substrate placed in a sol-gel mixture under hydrothermal conditions • time for film formation, 1-3 days
Properties of film	<ul style="list-style-type: none"> • low ordered mesostructures • random orientation of mesoporous channels 	<ul style="list-style-type: none"> • order mesoporous structure • vertically aligned channels perpendicular to the substrate surface 	

In this study, the EASA method was used to prepare MSFs on FTO glass slides, and, subsequently, used for immobilizing pyranine to develop an optical chemical sensor for PQ. The EASA method generates transparent MSFs suitable for UV-Vis spectroscopic and fluorometric studies. TEOS and sodium silicate were used as silica precursors. The films obtained from the two silica sources were compared. The as-synthesized films were incapable of directly immobilizing pyranine. Therefore, surface modification of the films was necessary.

Two methods can be used to modify the silica surface with aminosilane. The first method is a direct synthesis or co-condensation method, where aminosilane can be functionalized during the synthesis process of MSFs. Etienne et al. (2009) reported the synthesis of amine-functionalized MSFs by introducing 3-aminopropyltriethoxysilane (APTES) into the starting sol solution used for MSFs synthesis. The amount of APTES

should not exceed 10% of the silica precursor in the starting sol solution; otherwise, substantially disordered pore structures will be obtained. The second method is a post-synthesis or post-grafting method. The method involves adding MSFs into an APTES solution under suitable conditions (Ding et al., 2014; Lu et al., 2017). In this research, both methods were investigated for the functionalization of APTES on MSFs.



CHAPTER III

EXPERIMENTAL

3.1 Chemicals

Chemicals used in this research are listed in Table 3.1 and were used as received without any further purification.

Table 3.1 Chemicals used in this research.

Chemicals	Formula	Assay (%)	Suppliers
3-Aminopropyltriethoxysilane (APTES)	$C_9H_{23}NO_3Si$	99	ACRÖS
8-Hydroxypyrene-1,3,6-trisulfonic acid trisodium salt (Pyranine)	$C_{16}H_7Na_3O_{10}S_3$	96	Sigma-Aldrich
Acetone	CH_3COCH_3	99.8	Carlo Erba
Ammonia solution	NH_4OH	30	Carlo Erba
Disodium hydrogen phosphate anhydrous	Na_2HPO_4	99	QRëC
Ethyl alcohol absolute	C_2H_5OH	99.9	Carlo Erba
Ethylene diaminetetraacetic acid disodium salt, dihydrate	$C_{10}H_{14}N_2Na_2O_8 \cdot 2H_2O$	99	QRëC
Hexaammineruthenium (III) chloride	$Ru(NH_3)_6Cl_3$	99	Strem Chemicals

Table 3.1 Chemicals used in this research (Continued).

Chemicals	Formula	Assay (%)	Suppliers
Hexadecyltrimethylammonium bromide (CTAB)	$C_{19}H_{42}BrN$	99	ACRÖS
Hydrochloric acid	HCl	37	RCI Labscan
Methyl alcohol	CH_3OH	99.9	Carlo Erba
Methyl viologen hydrate or paraquat	$C_{12}H_{14}Cl_2N_2$	98	ACRÖS
Potassium hexacyanoferrate (III)	$K_3Fe(CN)_6$	99	Merck
Tetraethyl orthosilicate (TEOS)	$C_8H_{20}O_4Si$	98	Sigma-Aldrich
Silicon dioxide	SiO_2	Extra pure	Kemaus
Sodium hydroxide	NaOH	99	Carlo Erba
Sodium dihydrogen phosphate anhydrous	NaH_2PO_4	99	QRëC
Sodium nitrate	$NaNO_3$	99	Carlo Erba

3.2 Synthesis of mesoporous silica films

3.2.1 Stöber solution growth method

The preparation of mesoporous silica films (MSFs) using the Stöber solution growth method was carried out according to the literature (Teng et al., 2012). Fluorine-doped tin oxide (FTO) glasses (Yingkou Opv Tech New Energy) were placed in a Stöber solution containing 0.08 g of CTAB (0.22 mmol), 15 mL of ethanol, 35 mL of water, 5 μ L of concentrated ammonia aqueous solution, and 0.04 mL of TEOS (0.18 mmol), in a Teflon autoclave. The film growth was achieved under hydrothermal conditions at 60 °C for 72 hours. Afterward, the surfactant-silica films on the FTO glasses were rinsed with DI water, dried, and aged overnight in an oven at 100 °C. The surfactant was

removed by sonicating the films in an ethanol solution containing 0.1 M HCl for 10 minutes. The surfactant removal process was repeated three times.

The synthesis of MSFs using sodium silicate as a silica source was also studied. The same synthesis process was used, except that the synthesis mixture was composed of 0.08 g of CTAB (0.22 mmol), 15 mL of ethanol, 35 mL of water, 5 μ L of concentrated ammonia aqueous solution, and 0.023 g of Na_2SiO_3 (0.18 mmol).

3.2.2 Electrochemically assisted self-assembly method

The electro-assisted self-assembly (EASA) method from the literature (Walcarius et al., 2007) was used for synthesizing MSFs. A sol mixture consisting of 20 mL of ethanol, 20 mL of 0.1 M NaNO_3 , 2.84 g of TEOS (13.6 mmol), and 1.58 g of CTAB (4.35 mmol) (CTAB:TEOS ratio = 0.32) was prepared and stirred. The pH of the sol solution was adjusted to 3 using 0.1 M HCl (pH meter, EC30, Hach). The mixture was aged for 2.5 hours under stirring before use. The cleaned FTO glass, a working electrode, was then immersed in the sol mixture. A cathodic potential of -1.3 V was applied for a certain duration using a potentiostat (EMStat3+, PalmSens). Mesh stainless steel and silver/silver chloride (Ag/AgCl) electrodes were used as a counter electrode (CE) and a reference electrode (RE), respectively. The FTO glass was quickly removed from the solution after the potential application, rinsed with DI water, dried, and aged overnight in an oven at 130 °C. To create empty channels of mesoporous silica, CTAB was extracted using an ethanol solution containing 0.1 M HCl and sonicated for 10 minutes. The process was repeated three times.

The same procedure was applied for MSFs synthesis using sodium silicate as a silica source. The molar ratio of CTAB:Si in the sol mixture was kept at 0.32. However, in adjusting the mixture pH to 3, 8 M HCl was used instead. The mixture was aged for 2.5 – 24 hours with stirring before use. The cathodic potential of -1.3 V was applied in the time range of 300-900 seconds.

Multilayer films were prepared using the sequential EASA method described by Giordano et al. (2017). The cleaned FTO glass was immersed in the prepared sol mixture and a cathodic potential was applied at -1.3 V for 30 seconds for the formation of each layer, up to a total of four consecutive layers. Between each deposition cycle, the FTO glass was removed from the sol mixture and rinsed with DI water to prevent

the precipitation of silica aggregates. Once the deposition was completed, the multilayer film was aged overnight at 130 °C, followed by the removal of CTAB using the same procedure mentioned above.

3.3 Modification of MSFs with 3-aminopropyltriethoxysilane

Both monolayer and multilayer MSFs were functionalized with 3-aminopropyltriethoxysilane (APTES) using the post-synthetic method according to the literature (Ding et al., 2014). The MSFs were immersed in an ethanol solution containing APTES for 24 hours at 60 °C under refluxed conditions. The concentration of APTES used in the modification steps was 1, 3, and 5% v/v. The resulting modified MSFs were washed with acetone and ethanol and dried at 80 °C for 2 hours. The obtained films were denoted as NH₂-MSFs.

3.4 Immobilization of pyranine on NH₂-MSFs

To immobilize pyranine on NH₂-MSFs, the NH₂-MSFs were first immersed in 0.1 M HCl solution for 1 hour to protonate the amino groups in the film, followed by rinsing with DI water. The films were then immersed in a 1.0 mM pyranine solution. The resulting sensing films (Pyr-MSFs) were washed with DI water and left to dry at room temperature for 24 hours. The immobilization time was optimized to achieve the most suitable response signal.

3.5 Characterization of MSFs, NH₂-MSFs and pyranine-immobilized MSFs

The permeability and continuity of the films were assessed through cyclic voltammetric experiments, utilizing a 1.0 × 1.0 cm² Pt plate as a counter electrode, Ag/AgCl (Metrohm) as a reference electrode, and FTO glass as a working electrode, with a 0.1 M NaNO₃ solution as an electrolyte. Ru(NH₃)₆³⁺ and Fe(CN)₆³⁻ solutions were employed as electroactive probes. Cyclic voltammograms were recorded at a rate of 0.1 Vs⁻¹ for 5 scans at room temperature. The morphology of the films was visualized through a scanning electron microscope (SEM, JSM-6010LV, JEOL) and a transmission electron microscope (TEM, Talos F200X, Thermo Fisher Scientific). Phases of the films were characterized by an X-ray diffractometer (XRD, D8 advance, Bruker). Functional

groups on the films were identified via a Fourier transform infrared spectrometer (FTIR, Tensor27-Hyperion, Bruker) using an attenuated total reflectance mode. Finally, the performance of the sensing film in detecting paraquat in water and food samples was evaluated using a fluorescence spectrophotometer (LS 50 B, Perkin Elmer).

3.6 Response of sensing film to paraquat

Fluorescence spectroscopy was utilized to investigate the sensing film's response to paraquat. Prior to use, a sensing film was immersed in an ethanol-buffer solution pH 6.0 for 10 minutes. Fluorescence spectra were then recorded at an emission wavelength of 506 nm with an excitation wavelength of 450 nm. The fluorescence intensity measured with the sensing film in the ethanol-buffer solution was denoted as I_0 , and that in a PQ solution was denoted as I .

3.7 Calibration study for paraquat

At the optimal conditions, the sensing films were placed in standard PQ solutions of various concentrations, and fluorescence signals were recorded. The fluorescence quenching of pyranine by paraquat can be mathematically expressed by the Stern–Volmer Equation (3.1).

$$I_0/I = 1 + K_{SV}[Q] \quad (3.1)$$

In the Stern–Volmer Equation (1), I_0 represents the fluorescence intensity of the sensing film after being soaked in a buffer with a pH of 6.0 for 10 minutes, while I is the fluorescence intensity of the film after immersion in a paraquat solution. K_{SV} is the Stern–Volmer constant, and $[Q]$ represents the paraquat concentration. A calibration curve was generated by plotting $(I_0/I)-1$ against paraquat concentration using the Stern–Volmer plot.

3.8 Regeneration of sensing film

The regeneration of sensing films was investigated. Phosphate buffers pH 6.0 of various concentrations, including 0.01 M, 0.025 M, and 0.05 M, were used as regeneration agents. A sensing film was first immersed in a 10.0 ppm paraquat solution for 5 minutes and a fluorescence signal was recorded. After that, the film was soaked

in 10 mL of the regenerating reagent for 5-10 minutes, and washed with DI water. Finally, the sensing film was dipped in an ethanol-buffer solution pH 6.0 for 10 minutes and the fluorescence signal was recorded.

3.9 Reproducibility and repeatability

The reproducibility of the sensing film fabrication process was studied by measuring the fluorescence signal of sensing films prepared from ten batches of synthesized gel mixtures, each batch comprising five films. The reproducibility of the sensing films' responses to paraquat was evaluated by monitoring the fluorescence signals of five sensing films in a 5.0 ppm paraquat solution at 506 nm for 5 min.

The recycling capability of a sensing film was conducted by using one sensing film to measure the fluorescence signals of 3.0, 5.0, and 10.0 ppm paraquat solutions consecutively. The study was repeated with three sensing films.

3.10 Interference study

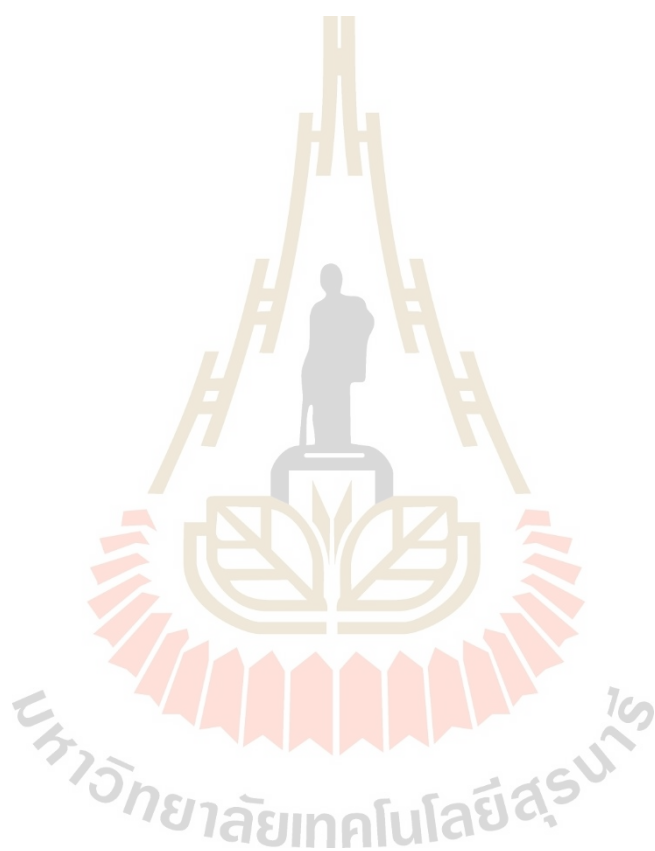
Influence of foreign species on the response of the sensing films to paraquat was studied. Cu^{2+} , Fe^{3+} , Zn^{2+} , K^+ , and carbaryl were chosen for this study. The measurements were conducted by measuring the fluorescence signals of the sensing films in a 10.0 ppm (3.90×10^{-5} M) paraquat solution with and without the tested species. The molar ratio of paraquat to the tested species was fixed at 1:5.

3.11 Analysis of real samples

The developed sensing films were employed to determine paraquat concentration in tap water and sugarcane peel samples. Tap water samples were collected from Suranaree University of Technology, Nakhon Ratchasima, Thailand. Sugarcane samples were collected from sugarcane fields in Nong Ruea, Khon Kaen Province, Thailand.

Before making measurements with the sensing films, extraction of paraquat in the samples was performed. Extraction procedures from previous reports (Kolberg et al., 2012; Pizzutti et al., 2016) were followed. For sugarcane peel samples, 25.0 g sample was refluxed with 100 mL of a mixture of methanol and 0.1 M HCl (1:1 v/v) at 80 °C

for 15 min. After cooling to room temperature, the liquid phase was separated by filtration through No.1 Whatman paper, adjusted to pH 6.0 using 10 M NaOH, and diluted to a total volume of 200 mL with DI water. Finally, 5.00 mL of the resulting liquid was treated with 0.5 mL of 5% EDTA and made up to 10.00 mL with a buffer solution. For tap water analysis, only pH adjustments were made to the samples. In a recovery study, paraquat was spiked into samples to obtain 10 ppm added paraquat samples.



CHAPTER IV

RESULTS AND DISCUSSION

Mesoporous silica films (MSFs) were explored as potential supporting materials for immobilizing 8-hydroxypyrene-1,3,6-trisulfonic acid trisodium salt, also known as pyranine. MSFs were chosen due to their high surface area, homogeneity, optical transparency, silanol surface capable of chemical modification, high water stability, and good film-forming properties. In this work, the Stöber solution growth method (Teng, 2012) and the electro-assisted self-assembly (EASA) method (Walcarius et al., 2007) were used to synthesize MSFs on fluorine-doped tin oxide (FTO) coated glass. The FTO glass is conductive and transparent, suitable for electrochemically and spectroscopically characterizing the synthesized materials. In the synthesis using the Stöber solution growth method, an FTO glass was placed in a synthesis gel and subjected to hydrothermal conditions at 60 °C for 72 hours. While in the synthesis using the EASA method involved applying a suitable cathodic potential to the FTO glass immersed in a hydrolyzed sol solution containing a silica source and surfactant in a water/ethanol acid solution. Tetraethyl orthosilicate (TEOS) and sodium silicate were investigated as silica sources for the MSFs synthesis via the EASA methods. Additionally, monolayer and multilayer MSFs synthesized using TEOS as a silica source were studied. The selected MSFs were modified with 3-aminopropyltriethoxysilane and immobilized with pyranine. Pyranine-immobilized MSFs were optimized and used for paraquat detection.

4.1 Characterization of MSFs from the Stöber solution growth method

Two silica sources, TEOS and sodium silicate, were used for synthesizing MSFs by the Stöber solution growth method to obtain films with pore channels aligned vertically perpendicular to the FTO glass surface. Figure 4.1 shows a picture and an SEM image of MSF synthesized using the Stöber solution growth method with TEOS as a silica source (MSF-ST). The obtained film appeared transparent but with slight turbidity, as shown in Figure 4.1a. A top-view SEM image of MSF-ST in Figure 4.1b reveals the formation of a thin film and the deposition of aggregate particles on the film surface.

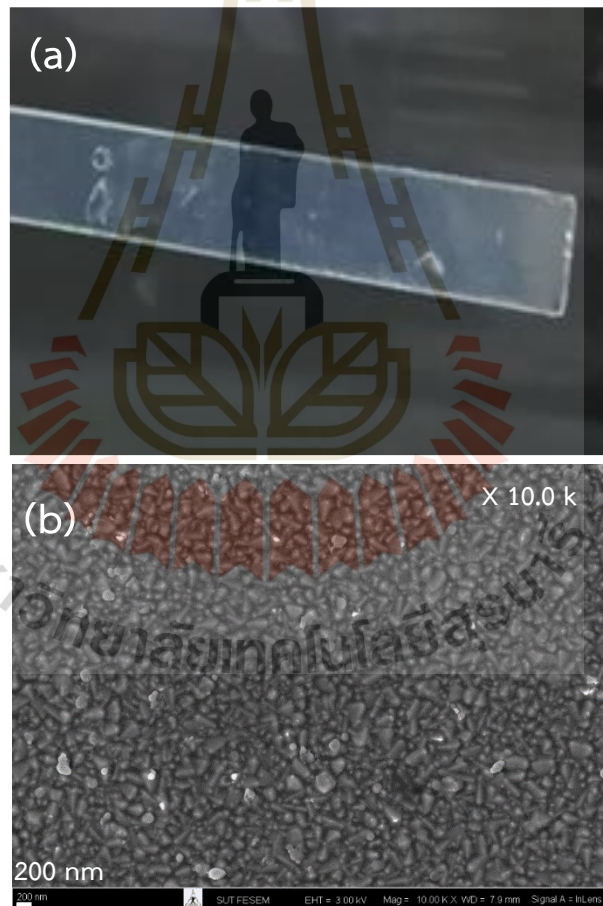


Figure 4.1 (a) A picture of the film synthesized by the Stöber solution growth method using TEOS as a silica source and (b) SEM image of the film.

The permeability of the pore channels was investigated using cyclic voltammetry (CV) with $\text{Ru}(\text{NH}_3)_6^{3+}$ as a redox probe (see Appendix A for a half-reaction involving the probe species). Figure 4.2 shows voltammograms obtained using MSF-ST as a working electrode immersed in the probe solution. Before the removal of CTAB, no redox signal was observed, indicating that the mesopore channels were blocked by the CTAB surfactant and resulting in no redox reaction at the electrode surface. The CV experiment confirms that the electrode surface was completely covered with the film without cracks. After removing CTAB from the mesopore channels, the film surface became negatively charged, allowing the cationic redox probe to access the electrode surface and produce a signal.

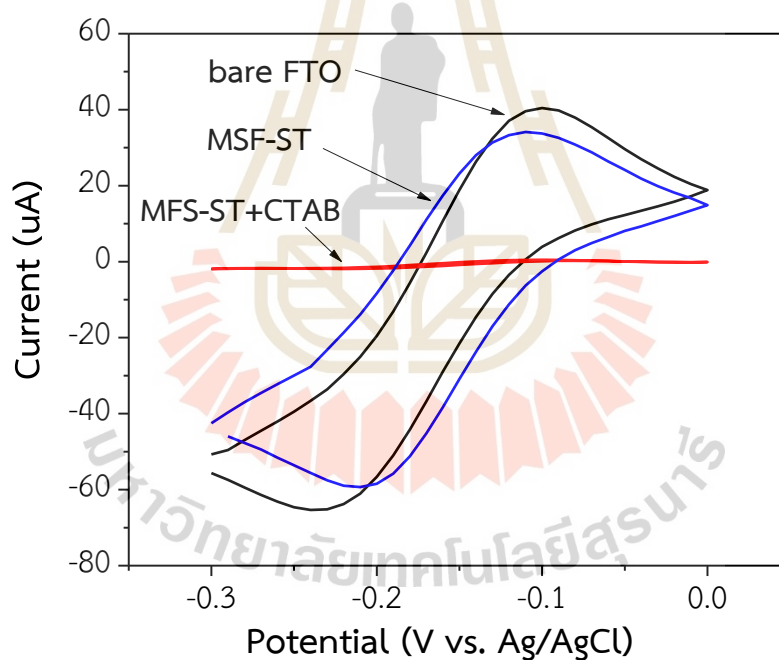


Figure 4.2 Cyclic voltammograms of bare FTO electrode and MSF-ST/FTO electrode before and after surfactant removal recorded in a solution containing 0.5 mM $\text{Ru}(\text{NH}_3)_6^{3+}$ and 0.1 M NaNO_3 . The scan rate was 0.1 Vs^{-1} . The electrode size is $0.9 \times 0.9 \text{ cm}$.

In the synthesis using sodium silicate as a silica source, no film was observed on the FTO glass. Figure 4.3 shows similar cyclic voltammogram patterns of the FTO electrode before and after the synthesis. The results confirm that the film was not successfully formed on the FTO glass.

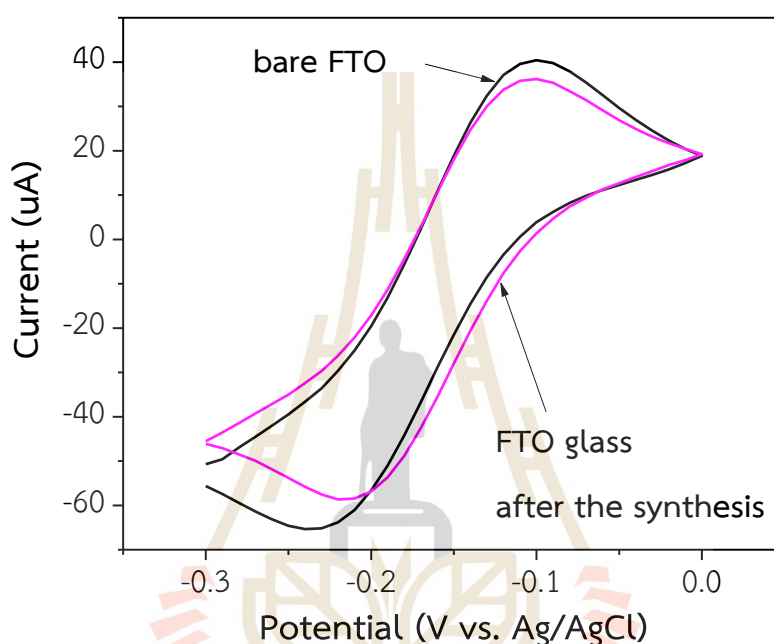


Figure 4.3 Cyclic voltammograms of the FTO electrode before and after the synthesis using sodium silicate as a silica source. The same conditions for voltammetric measurements as in Figure 4.2 were used.

The Stöber solution growth method was successfully used for synthesizing MSFs on FTO glass from TEOS as the silica source. However, the method requires a significantly long time of 72 h to form the thin films. In addition, it is challenging to synthesize films with higher thicknesses. The method was, therefore, not used further to fabricate sensing films.

4.2 Characterization of MSFs synthesis via the EASA method

4.2.1 Characterization of MSFs obtained from TEOS as silica source

MSFs were synthesized by applying a potential of -1.3 V at various times, 30, 60, 120, 180, and 300 seconds. The films synthesized via the EASA method using TEOS as a silica source were designated as MSF-EASA-TEOS. Figure 4.4 shows the synthesized films. The films appeared more turbid when the potential application time was increased. Additionally, characterization through CV experiments and SEM revealed notable characteristics.

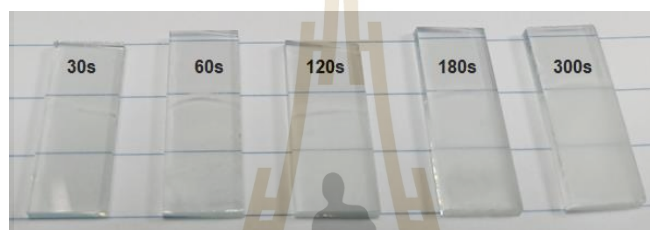


Figure 4.4 Photographic image of MSFs/FTO at various deposition times. The surfactant on the films was removed.

Figure 4.5 shows cyclic voltammograms of the FTO glass before and after the synthesis. Prior to the removal of CTAB, no redox signal of $\text{Ru}(\text{NH}_3)_6^{3+}$ was observed, indicating the blockage of mesopore channels by CTAB. This observation confirms that the film completely covered the electrode surface without cracks. Following the CTAB removal from the mesopore channels, the cationic redox probe could access the electrode surface producing a signal. Conversely, when $\text{Fe}(\text{CN})_6^{3-}$ was used as a probe, no signal was observed. This suggests that the pore had a negative polarity (Ding et al., 2014), which repulsed the anionic redox probe from diffusing to the electrode surface.

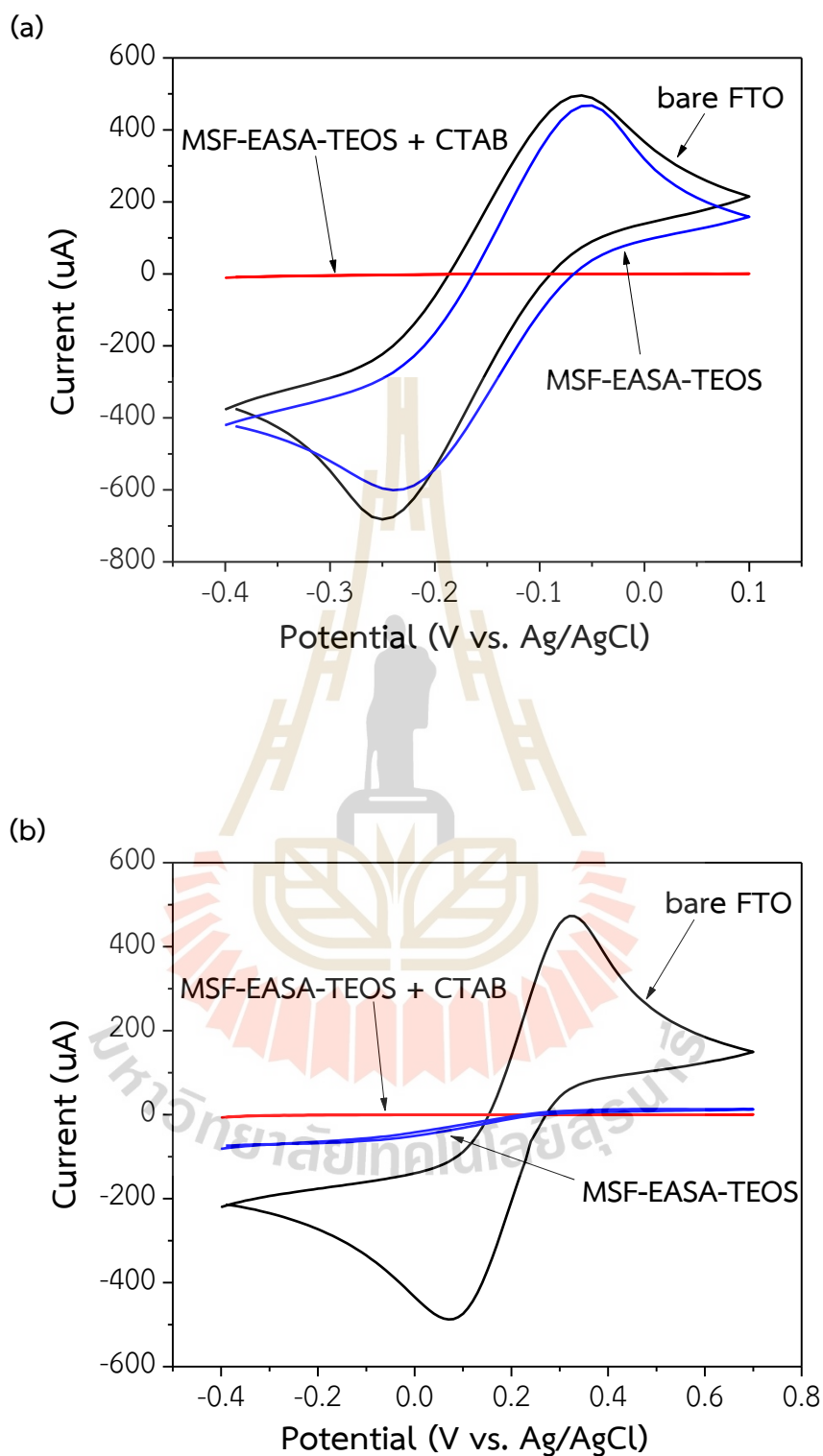


Figure 4.5 Cyclic voltammograms of MSF-EASA-TEOS/FTO electrodes recorded in 0.1 M NaNO₃ solutions containing (a) 5.0 mM Ru(NH₃)₆³⁺ and (b) 5.0 mM Fe(CN)₆³⁻. The scan rate was 0.1 Vs⁻¹.

Figure 4.6 displays the FTIR spectra of MSFs-EASA-TEOS both before and after surfactant removal. The observed bands at 2970 and 2890 cm^{-1} were assigned to the aliphatic C-H stretching of CTAB. Following the surfactant removal, these vibration bands disappeared, indicating the complete removal of CTAB from MSFs through extraction in ethanol containing 0.1 M HCl for 10 minutes. These results confirm the efficacy of the extraction process in eliminating CTAB from MSFs.

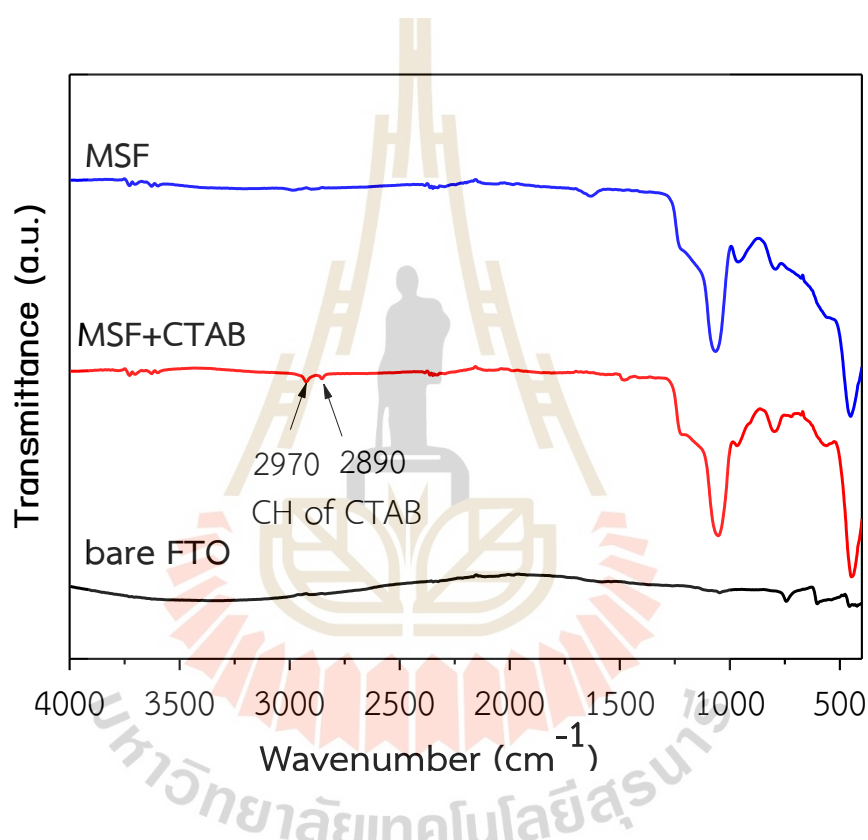


Figure 4.6 FTIR spectra of MSF-EASA-TEOS/FTO glass, before/after surfactant removal and on bare FTO electrode.

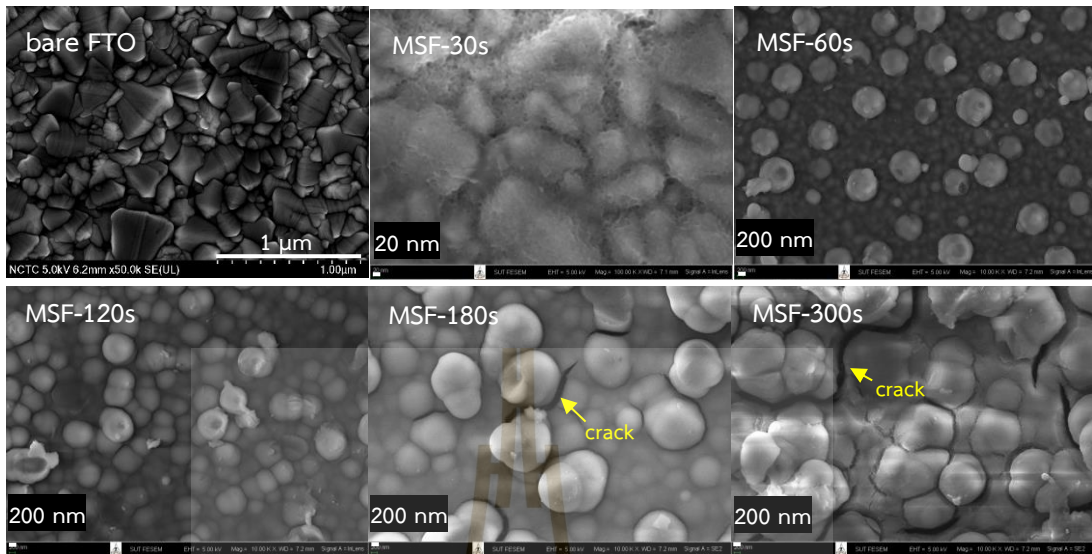
MSFs were synthesized using a -1.3 V potential and different deposition times to vary the film thickness. The deposition times included 30, 60, 120, 180, and 300 seconds and the obtained films were designated as MSF-30s, MSF-60s, MSF-120s, MSF-180s, and MSF-300s, respectively. SEM and TEM were used to obtain the morphology of the synthesized films. Figure 4.7 shows the SEM images revealed the presence of particles on the thicker films. Figure 4.7a displays top-view SEM images of

MSF with various deposition times. A thin film of MSFs was deposited on the FTO surface with an initial deposition time of 30 seconds. The film became thicker as the deposition time increased and silica aggregates were also observed. The silica particle size ranges from 600 nm to 900 nm in diameter. Furthermore, after more than 60 seconds of deposition, some silica particles were observed to be embedded within the film. Therefore, the synthesis film thickness depends on the deposition time. Figure 4.7b shows that the thickness of MSF-60s, MSF-180s, and MSF-300s was 172 nm, 520 nm, and 1.2 μm , respectively. However, cracks were observed in the MSF-180s and MSF-300s films.

The results of the CV experiments, as shown in Figure 4.8, were also corroborating with the film morphology. The redox current decreased with increased deposition time compared to the bare FTO electrode due to the limitation of the mass transport through the films due to the thickness and particle aggregation, resulting in a slower transport rate, as previously reported (Goux et al., 2009, Nasir et al., 2019). Therefore, MSF-60s was chosen as the supporting matrix for the subsequent experiments because it provided relatively thick, transparent films with a few evenly distributed particles.

TEM images of the silica film, removed from the FTO glass and deposited on a TEM grid, are shown in Figure 4.9. The results demonstrate that the silica film has a hexagonal packing of mesopores with nanochannels approximately 5 nm in diameter.

a) top view



b) cross-section



Figure 4.7 SEM images of MSFs/FTO from different deposition times a) top view and b) cross-section.

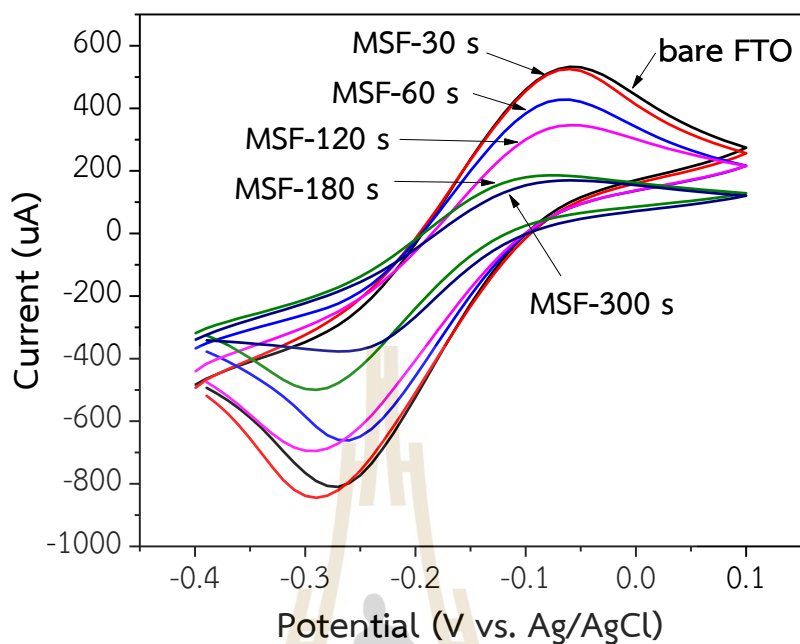


Figure 4.8 MSFs synthesized from various deposition times and surfactant removed; CVs recorded in a solution containing 5 mM $\text{Ru}(\text{NH}_3)_6^{3+}$ and 0.1 M NaNO_3 . MSFs-T/FTO and on bare FTO electrode; scan rate 0.1 Vs^{-1} , the electrode size is $0.9 \times 0.9 \text{ cm}$.

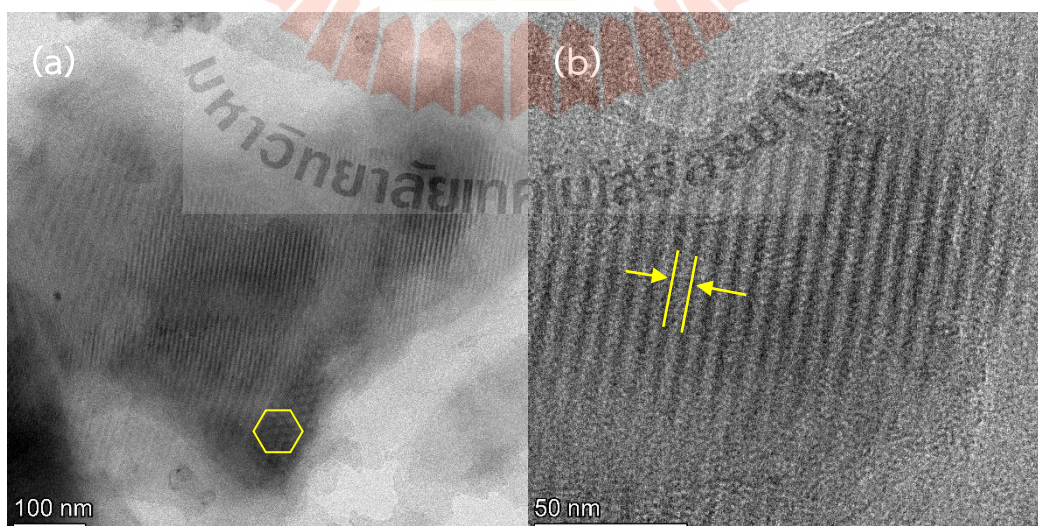


Figure 4.9 TEM images of MSFs peeling off from FTO substrate.

4.2.2 Characterization of MSFs obtained from sodium silicate as silica source

TEOS is commonly used as the silica source in MSF synthesis. However, the price of TEOS is relatively high. Therefore, sodium silicate was investigated as an alternative silica source for MSF synthesis. The EASA method was used. Sodium silicate concentration, hydrolysis time, and deposition time were studied.

Figure 4.10 show CV voltammograms of the material synthesized under the following conditions: Na_2SiO_3 content 6.7, 10.5, or 13.6 mmol while maintaining a constant mole ratio of CTAB to Na_2SiO_3 at 0.32, hydrolysis time 15 h, and deposition time 900 seconds. CTAB was not removed from the electrodes in the CV measurements. The results showed that the redox currents were observed from the electrodes synthesized using 6.7 and 10.5 mmol of Na_2SiO_3 compared with the bare FTO electrode, indicating that the film did not adequately cover the electrode surface. However, at 13.6 mmol of Na_2SiO_3 , only a small redox current was observed. The result implies better film coverage on the electrode surface. However, the precipitation of silica occurred in the hydrolyzed sol. The XRD pattern in Figure 4.10b shows a broad band around 2θ of 23° which is amorphous silica (Suwannaboot et al., 2023).

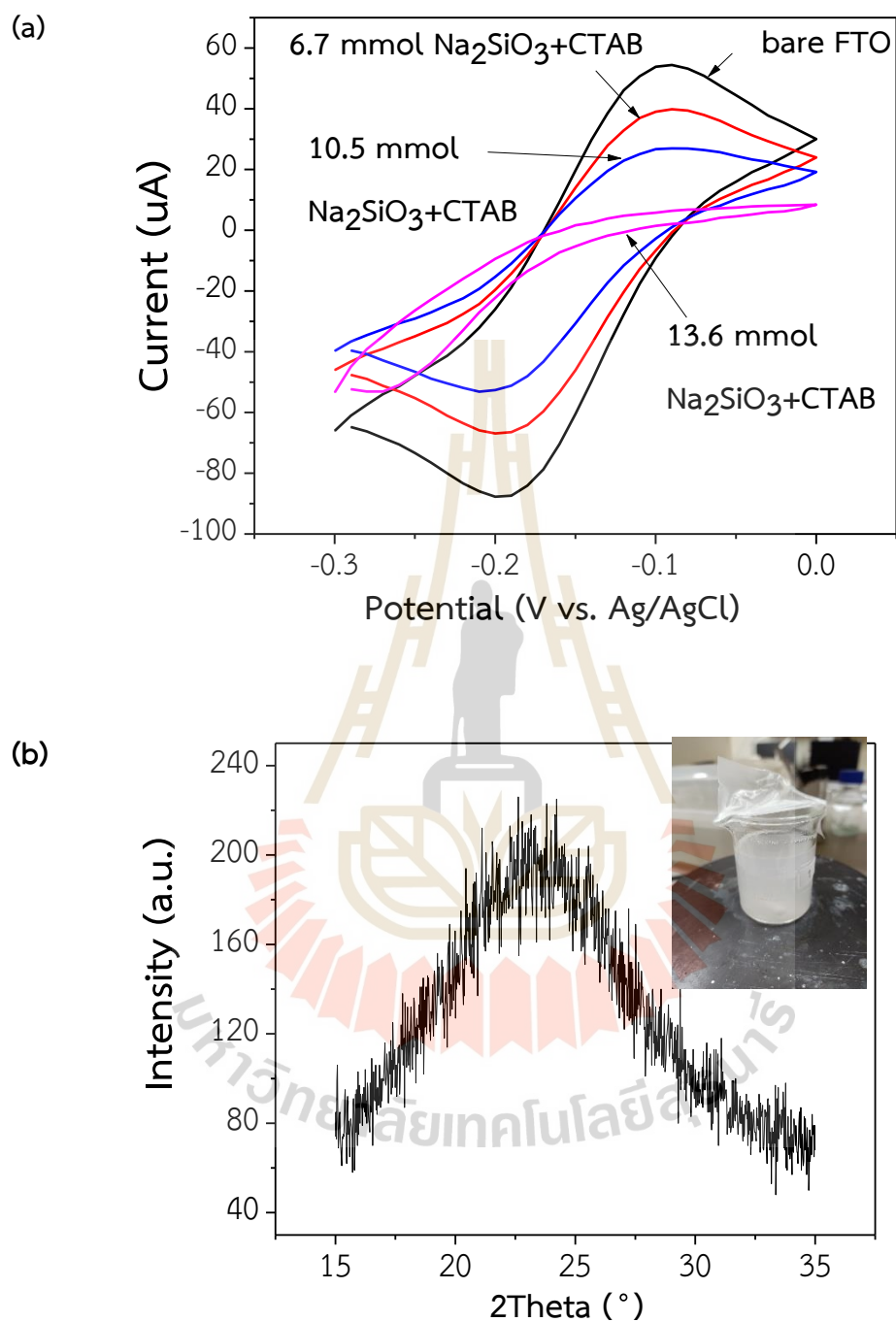


Figure 4.10 (a) Cyclic voltammograms of the electrodes synthesized with different Na_2SiO_3 content without surfactant removal recorded in a solution containing 5 mM $\text{Ru}(\text{NH}_3)_6^{3+}$ and 0.1 M NaNO_3 (b) XRD pattern of the silica particles, an inset shows a picture of the hydrolyzed sol.

Figure 4.11 shows voltammograms of the materials from the synthesis under the following conditions; the hydrolysis time at 2.5, 15, or 24 h, 13.6 mmol of Na_2SiO_3 , a constant mole ratio of CTAB to Na_2SiO_3 at 0.32, and deposition time of 900 seconds. The experimental findings indicate that the electrode surface coverage resulted from synthesis under the 15 and 24-hour hydrolysis conditions. However, the transparent film obtained from these conditions exhibited a slight presence of redox current, which might be attributed to potential factors such as incomplete coverage or the occurrence of cracks within the film.

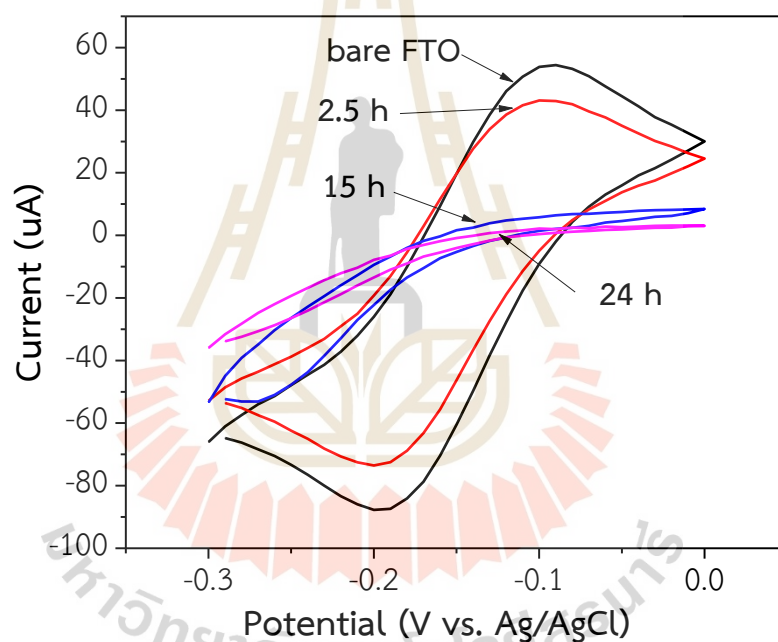


Figure 4.11 Cyclic voltammograms of the electrodes synthesized with different hydrolysis times without surfactant removal recorded in a solution containing 5 mM $\text{Ru}(\text{NH}_3)_6^{3+}$ and 0.1 M NaNO_3 .

Figure 4.12 shows voltammograms of the materials from the synthesis under the following conditions; the deposition time at 300, 600, or 900 seconds, 13.6 mmol of Na_2SiO_3 , a constant mole ratio of CTAB to Na_2SiO_3 at 0.32, and hydrolysis time 15 h. The results showed that the redox current decreased as the deposition time increased, compared to the bare FTO electrode. Additionally, the redox current of the film was observed a slight presence at 900 s. This suggests that a silica film can form on the electrode surface as a thin film, but it requires a longer deposition time.

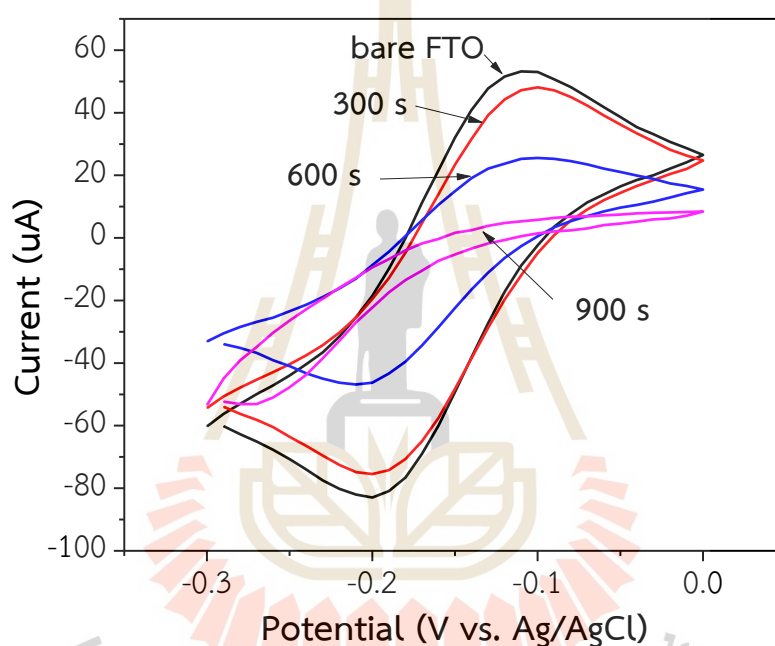


Figure 4.12 Cyclic voltammograms of the electrodes synthesized with different deposition times without surfactant removal recorded in a solution containing 5 mM $\text{Ru}(\text{NH}_3)_6^{3+}$ and 0.1 M NaNO_3 .

Figure 4.13 shows the SEM image of thin film on FTO synthesized with initial 13.6 mmol Na_2SiO_3 at a constant mole ratio of CTAB to Na_2SiO_3 of 0.32, a hydrolysis time of 15 h, and a deposition time of 900 seconds. The image reveals that a silica film has been successfully deposited onto the FTO glass.

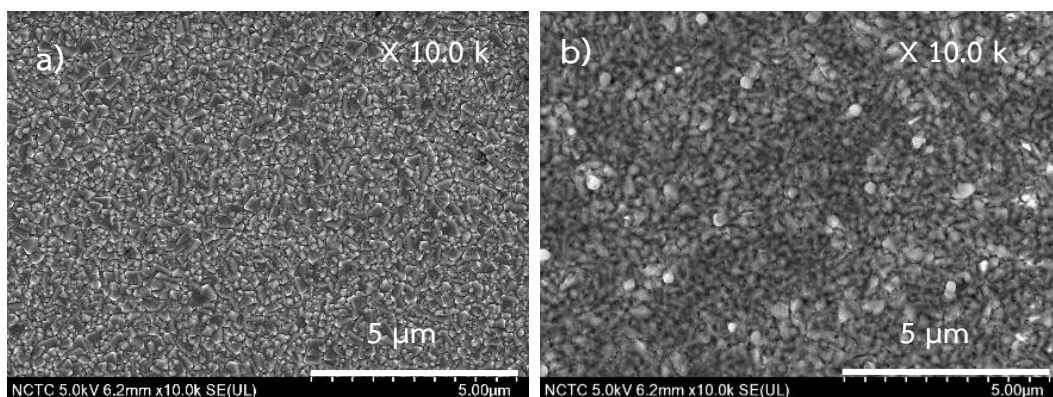


Figure 4.13 SEM images of a) bare FTO b) thin film on FTO.

To summarize, the synthesis of MSFs with sodium silicate as the silica source using the EASA method was explored. The formation of silica films was observed at particular synthesized conditions; however, the films seemed thin compared to those obtained from the synthesis using TEOS. Incomplete film deposition and cracks may have occurred, rendering the film unsuitable for use as support for fabricating sensing films.

4.3 Characterization of the multilayer films obtained from using tetraethyl orthosilicate as silica source

One strategy to increase the amount of immobilized sensing reagent is to increase the film thickness. This research synthesized the thicker MSF via the EASA method according to the literature (Giordano et al., 2017). This method applied the potential intermittently to deposit a single-layer film at a time and kept repeating to obtain a multilayer film. The deposition time of 30 s was used for synthesizing each layer. Multilayer MSF synthesized using TEOS as a silica source was designated as mMSF-TEOS. The morphology analysis of the mMSF-TEOS was conducted using scanning electron microscopy (SEM) and the results are shown in Figure 4.14. These images reveal that thicker films have more silica aggregates than monolayer film, which agrees with the literature (Giordano et al., 2017).

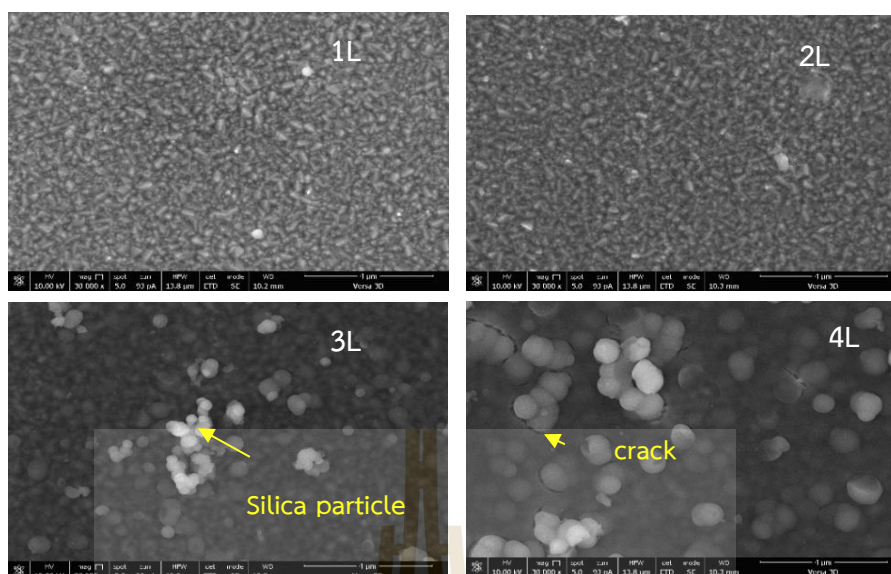


Figure 4.14 SEM images of mMSF-TEOS /FTO. xL indicates the number of deposition layers where x = 1, 2, 3 or 4.

A CV analysis was performed using $\text{Ru}(\text{NH}_3)_6^{3+}$ as the cationic redox probe. Before the removal of CTAB, no redox signal was observed, as shown in Figure 4.15. However, after the CTAB removal, the current decreased as the number of film layers increased. This decrease can be attributed to the limitation of mass transport through the films, resulting in a slower transport rate.

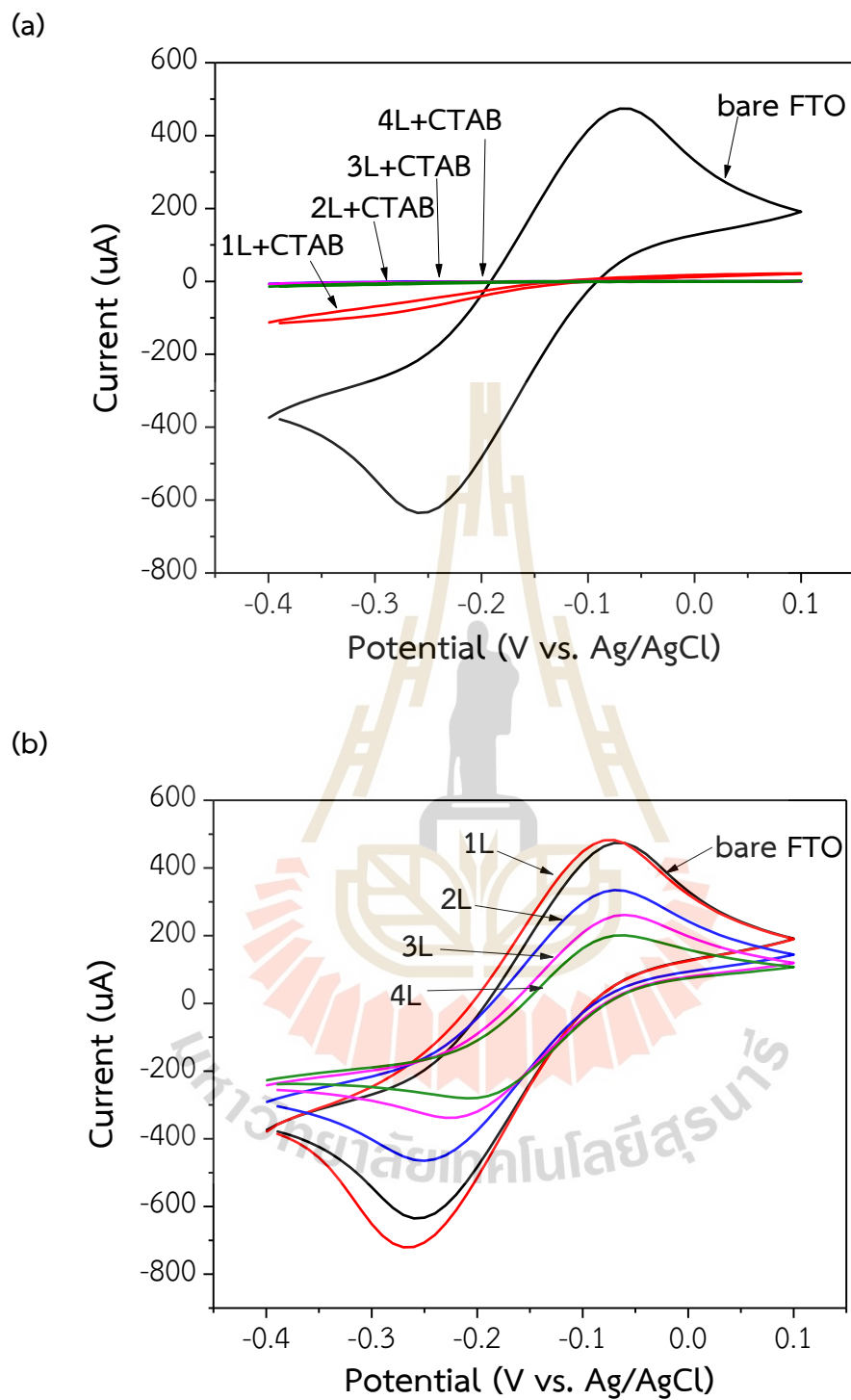


Figure 4.15 Cyclic voltammograms of 5 mM $\text{Ru}(\text{NH}_3)_6^{3+}$ redox probe in 0.1 M NaNO_3 solution on mMSF-TEOS/FTO, before (a) and after (b) surfactant removal; scan rate: 0.1 mVs^{-1} , electrode area: 0.9 \times 0.9 cm.

It is worth noting that the Stöber method could deposit silica films onto FTO among the synthesis procedures when TEOS was used as a silica source. However, turbid films were obtained, and the method required a long synthesis time. MSF could not be successfully synthesized using sodium silicate as a silica source using the Stöber method under the same experimental conditions. While the EASA method successfully produced mesoporous films on FTO using TEOS and sodium silicate as silica sources. The films synthesized by the EASA method using TEOS as a silica source were further used for the sensor fabrication.

4.4 Characterization of mesoporous silica films modified with 3-aminopropyltriethoxysilane

The modification of MSFs was performed by soaking MSFs with CTAB removed in a 3-aminopropyltriethoxysilane (APTES) solution in ethanol at 60 °C for 24 hours (Ding et al., 2014). The modified films were subsequently washed with acetone and ethanol and dried at 80 °C for 2 hours. The concentration of APTES used in the modification process varied in the range of 0-5% (v/v). The APTES-modified MSF was designated as NH₂-MSF.

4.4.1 Functional groups analysis of NH₂-MSF by FTIR

FTIR analysis was used to confirm the successful grafting of aminopropyl groups on the MSFs. FTIR spectra of aminopropyl-modified MSF with 1%, 3% and 5% v/v APTES are presented in Figure 4.16. The bands at 2977 cm⁻¹ and 2893 cm⁻¹ correspond to the aliphatic C-H stretching of aminopropyl of APTES. The bending vibration of N-H (primary amine) is observed at 1520 cm⁻¹ and a strong band at 1398 cm⁻¹ for the combination of stretching C-N of primary amides is also seen. The stretching of the Si-O-Si band peaks at 1066 cm⁻¹ (Farook et al., 2010, Majoul et al., 2015). The peak intensity of the amine group at 1520 cm⁻¹ is observed to increase with increasing APTES concentration, which is consistent with the results of CV experiments. These findings provide evidence that amino groups have been successfully functionalized on the surface of MSFs.

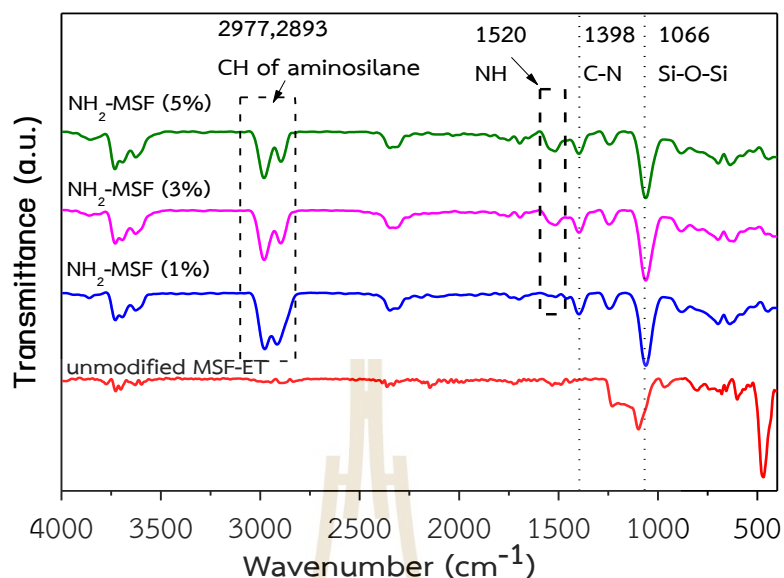


Figure 4.16 FTIR spectra of NH_2 -MSF from various concentrations of APTES used in the modification.

4.4.2 Permeability of NH_2 -MSF by cyclic voltammetry

The mass transport properties of the modified mesoporous silica films (MSFs) were investigated using cyclic voltammetry (CV) with $\text{Ru}(\text{NH}_3)_6^{3+}$ and $\text{Fe}(\text{CN})_6^{3-}$ as electroactive probes. The results are shown in Figure 4.17. After modification of the MSFs with APTES and protonation in an acidic solution, the surface of the modified MSFs became positively charged. When studied with the cationic probe, the signals from the modified films were lower than those from the unmodified film as shown in Figure 4.17a. The repulsive electrostatic interaction between the protonated amino groups on the MSFs and the $\text{Ru}(\text{NH}_3)_6^{3+}$ ions could contribute to such results. The signal responses of $\text{Ru}(\text{NH}_3)_6^{3+}$ on the modified MSFs decreased with increasing APTES concentration, indicating that the amine-functionalized MSFs became less permeable with higher APTES concentrations. Conversely, the current signal of the study using anionic redox probe ($\text{Fe}(\text{CN})_6^{3-}$) in Figure 4.17b displayed a high response from the amino-modified MSFs compared to that of the unmodified MSF (Ding et al., 2014). The signal responses of $\text{Fe}(\text{CN})_6^{3-}$ on the modified MSFs decreased with increasing APTES concentration.

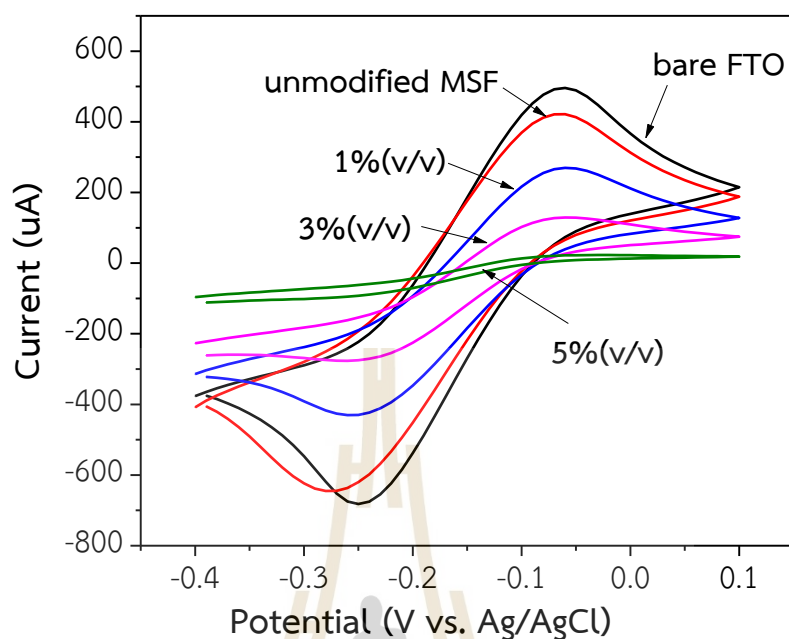
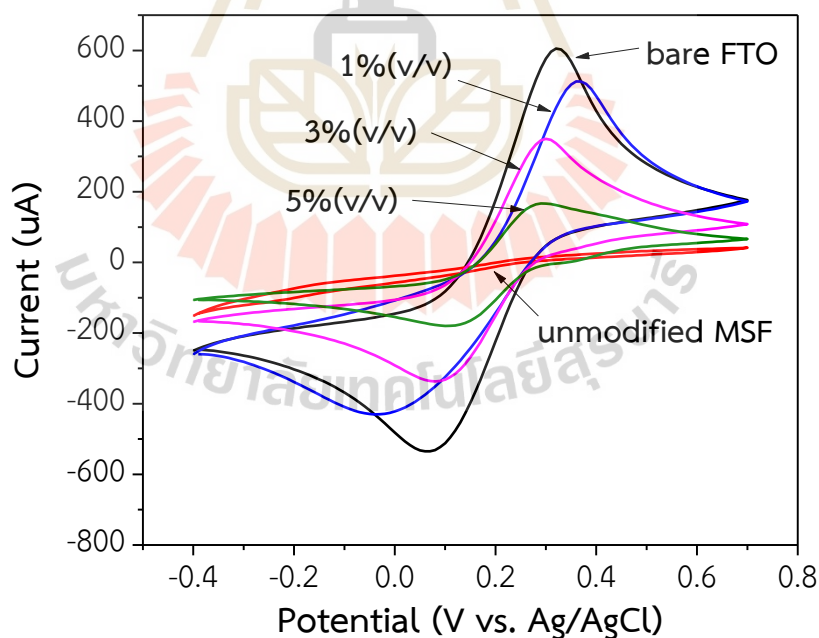
a) $\text{Ru}(\text{NH}_3)_6^{3+}$ b) $\text{Fe}(\text{CN})_6^{3-}$ 

Figure 4.17 Cyclic voltammograms of a) 5 mM $\text{Ru}(\text{NH}_3)_6^{3+}$ and b) 5 mM $\text{Fe}(\text{CN})_6^{3-}$ redox probe in 0.1 M NaNO_3 solution on modified MSFs with various concentrations of APTES, on MSF and on bare FTO electrode; Scan rate 0.1 Vs^{-1} , the size of the electrode is $0.9 \times 0.9 \text{ cm}$.

The same conditions used for modifying monolayer MSFs were applied for modifying multilayer MSFs with 3%APTES at 60 °C for 24 hours. The mass transport of the modified-multilayer MSFs was characterized by a CV experiment using $\text{Fe}(\text{CN})_6^{3-}$ as an anionic redox probe, shown in Figure 4.18. The results showed that the signal responses of the modified multilayer MSFs decreased with increasing layers, indicating high amine content in the multilayer.

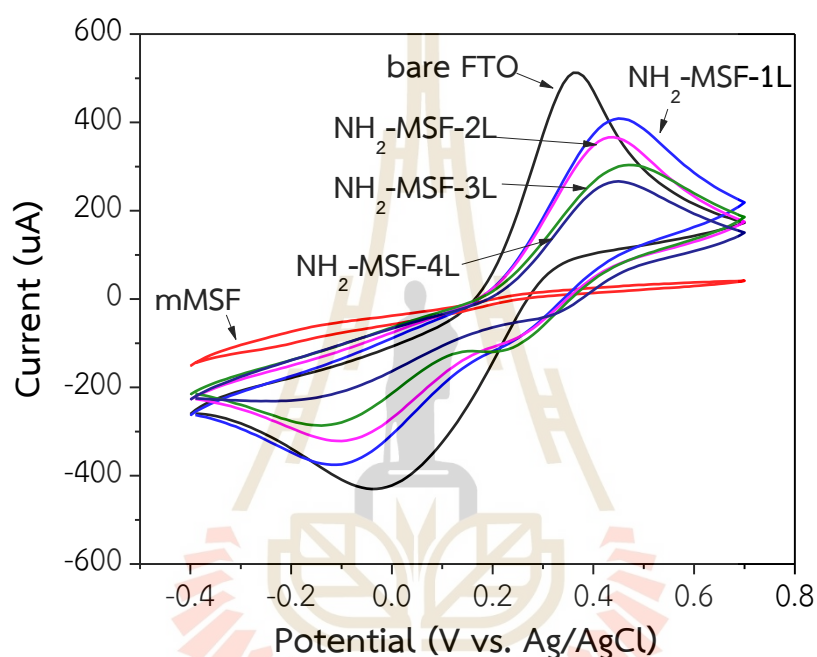


Figure 4.18 Cyclic voltammograms of 5 mM $\text{Fe}(\text{CN})_6^{3-}$ redox probe in 0.1 M NaNO_3 solution on NH_2 -multilayer MSF; Scan rate 0.1 mVs^{-1} , the size of the electrode is $0.9 \times 0.9 \text{ cm}$.

4.5 Immobilization of pyranine on MSFs

Pyranine (Pyr) was used as a sensing reagent for paraquat, which could be monitored spectrometrically. To immobilize pyranine on amino-grafted MSFs, the modified MSF must be protonated in an acid solution before immersing the film in a pyranine solution. The immobilization was conducted by immersing the protonated film (modified with 3%APTES) into a 1 mM pyranine solution for 12 hours. The color of the obtained film was light yellow as shown in Figure 4.19, The pyranine-immobilized film, designated as Pyr-MSF, showed a fluorescence emission at 506 nm

when excited at 450 nm. The dye could be immobilized on the film through an ionic interaction between the sulfonic groups of pyranine and the protonated aminopropyl on the silica surface.

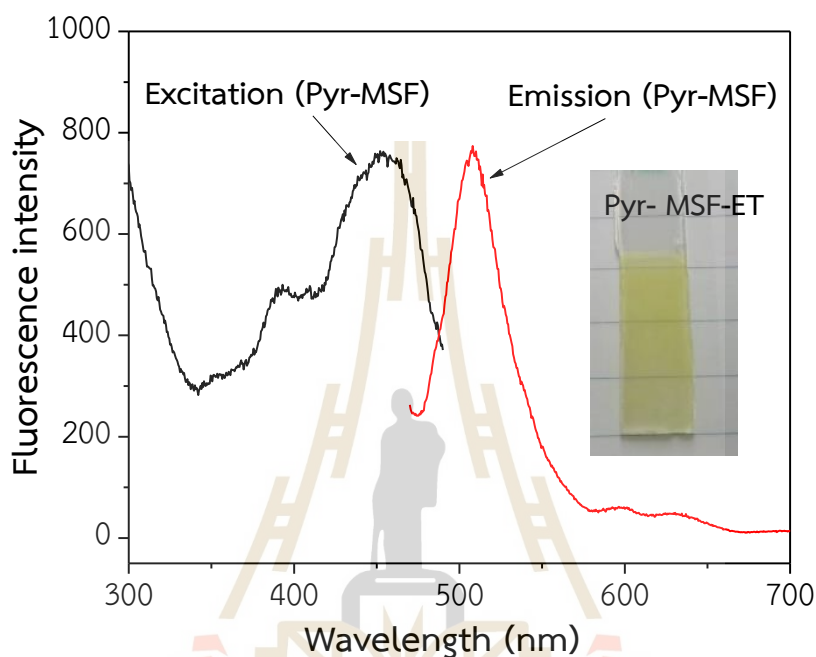


Figure 4.19 Fluorescence spectra of pyranine immobilized on MSF and a photograph of the film.

Multilayered-MSFs were also investigated in the immobilization of pyranine using the same immobilization conditions as that for the monolayer MSF. The pyranine-immobilized MSFs show similar emission spectrum patterns, as illustrated in Figure 4.20a. The fluorescence intensity tended to increase with the number of layers of MSFs due to more immobilized pyranine in the film. However, when the film thickness increased, pyranine seemed not to distribute evenly on the films, as shown in Figure 4.20b. The monolayer MSF appeared to have a more homogeneous distribution of pyranine; therefore, it was selected for further study.

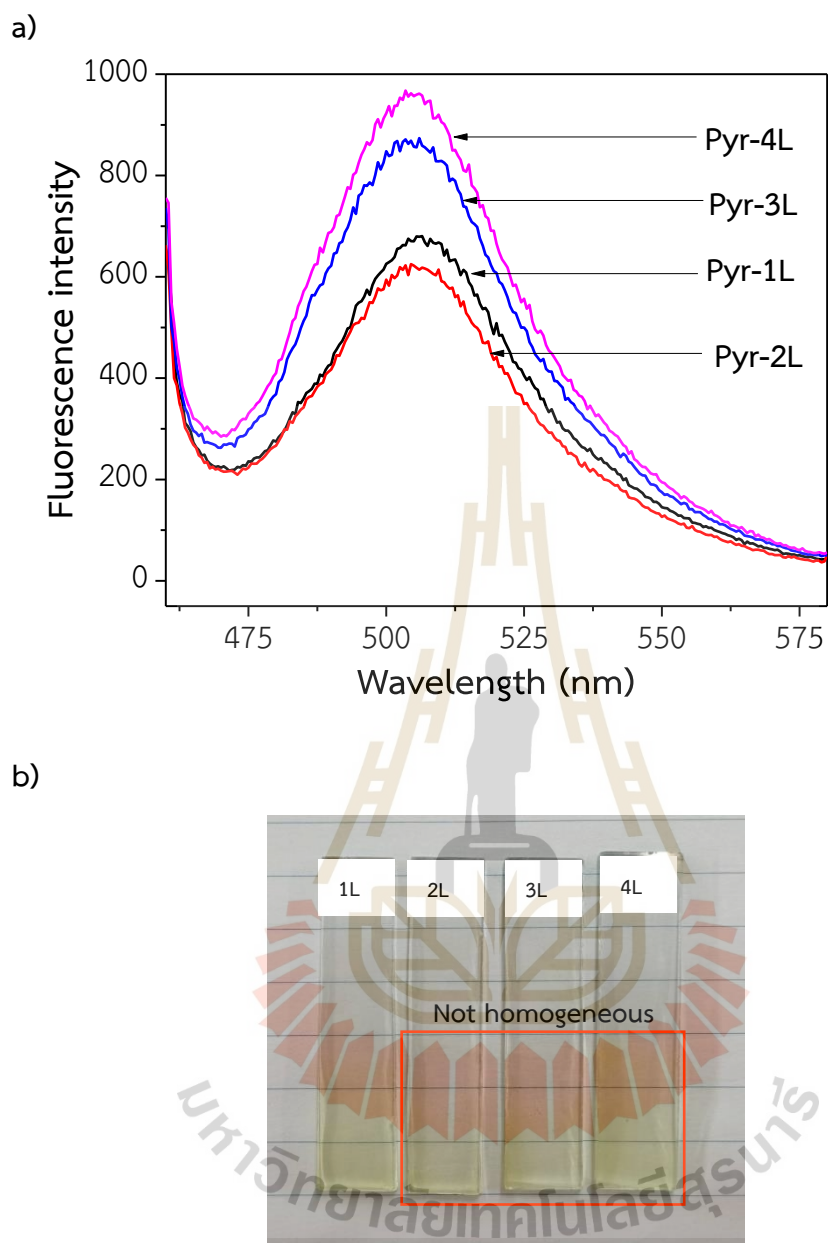


Figure 4.20 a) Fluorescence spectra of monolayer MSF and multilayered-MSFs b) a photograph of pyranine immobilized films.

4.6 Optimization of sensing films

The monolayer MSFs, which used TEOS as the silica source, were selected as the supporting material for immobilizing pyranine due to their homogeneity, optical transparency, good film-forming properties, and suitability for dye immobilization.

4.6.1 Effect of APTES concentration on the immobilization of pyranine

Pyranine was immobilized on MSFs after modification with different APTES concentrations. Figure 4.21 shows that the fluorescence intensity at 506 nm increased with increasing APTES concentration when the films were soaked in a buffer pH 6.0. The increase in fluorescence signals was likely due to a higher aminopropyl content in the films. However, the fluorescence intensity of the 5%-APTES-modified film was off-scale, and pyranine was leached slightly into the solution. Therefore, a 3%-APTES-modified film was chosen for further study.

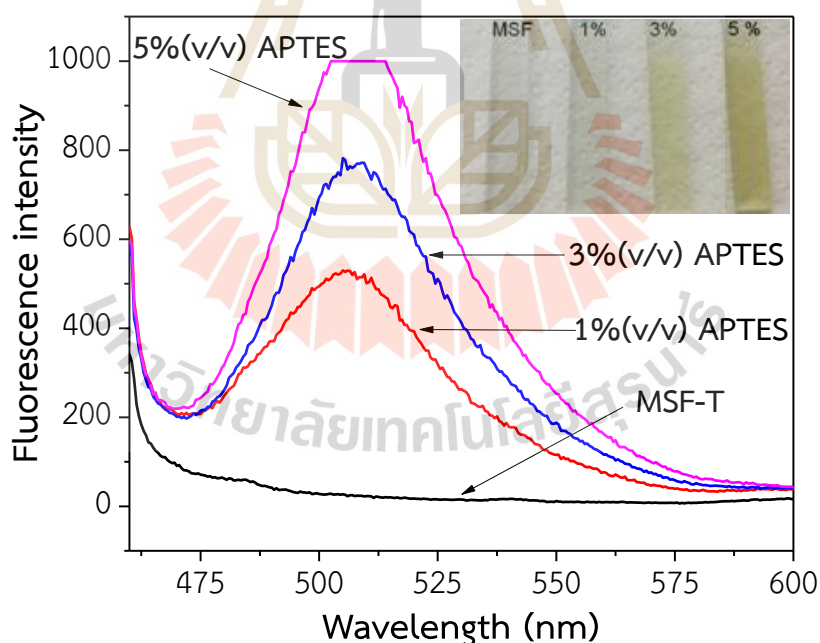


Figure 4.21 Fluorescence spectra of sensing films modified with various APTES concentrations in buffer pH 6.0.

4.6.2 Time for pyranine immobilization

The time for pyranine immobilization was varied from 1 to 24 hours to obtain the optimum fluorescence signal of pyranine. The fluorescence intensity of pyranine-immobilized films at 506 nm was monitored, and the results showed that the fluorescence response increased with increasing soaking time. The maximum response became stable after 12 hours, as shown in Figure 4.22.

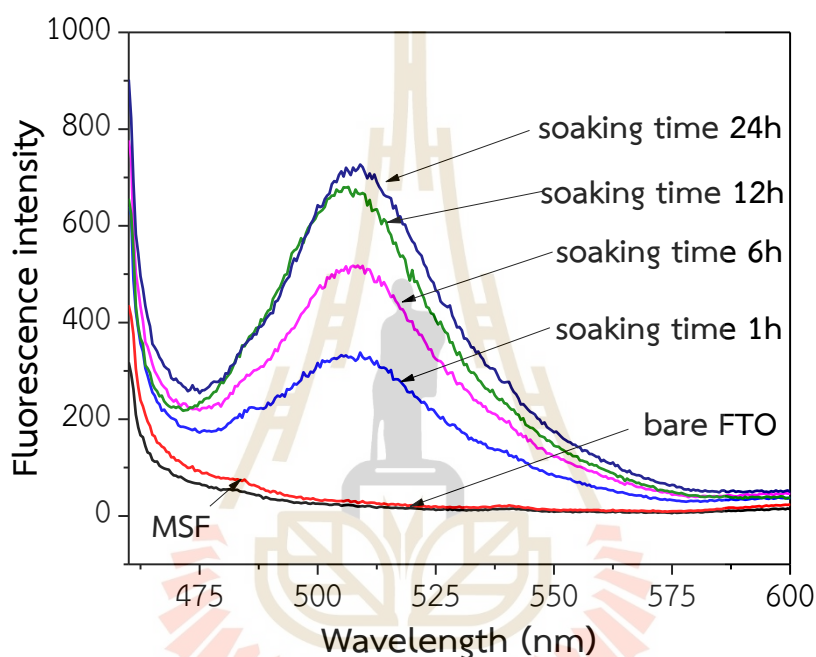


Figure 4.22 Fluorescence spectra of sensing films at various immobilization times.

4.6.3 Effect of pH on the fluorescence of pyranine-immobilized film

Ethanol was used as a solvent to prepare buffers to minimize pyranine leaching in solutions. The reason for this is that the solubility of pyranine is much lower in ethanol than in water. The effect of solution pH on the fluorescence signal was studied by immersing the films into a 9:1 v/v ethanol/DI water buffers with a pH ranging from 4.0 to 7.0. The fluorescence intensity was monitored 10 minutes after placing the film in the solution. The results in Figure 4.23 show that the fluorescence intensity at 506 nm increased with increasing pH. The maximum response was obtained at pH 7.0. However, pyranine leached out from the sensing film into the buffer at this pH. When

conducted the experiment at pH 6.0, no significant pyranine leaching was observed. Therefore, the pH of sample solutions in the further study was kept at this pH.

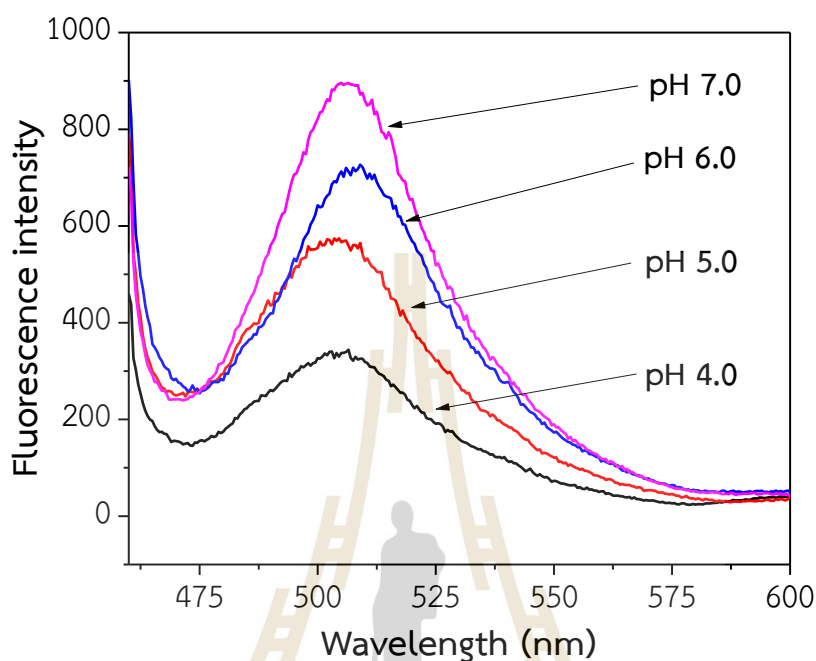
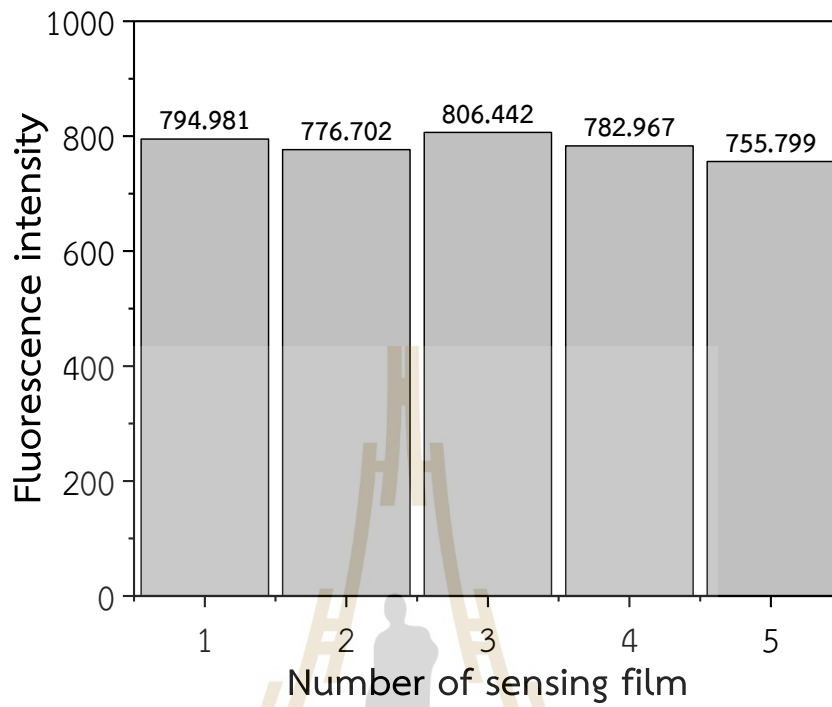


Figure 4.23 Fluorescence spectra of sensing films in buffer at different pH.

4.6.4 Reproducibility of sensing film fabrication

The reproducibility of the sensing film fabrication procedure was assessed by measuring the fluorescence intensity at 506 nm from ten batches of synthesized gel mixture, each comprising five films. The results are presented in Figure 4.24. Figure 4.24a shows that the signals from five films were about the same, with a relative standard deviation (RSD) of 2.4%. When making measurements with the films prepared from ten batches of synthesized sol-gel mixtures, the RSD was 7.1% as shown in Figure 4.24b. The results suggested that the fabrication procedure was reproducible.

a)



b)

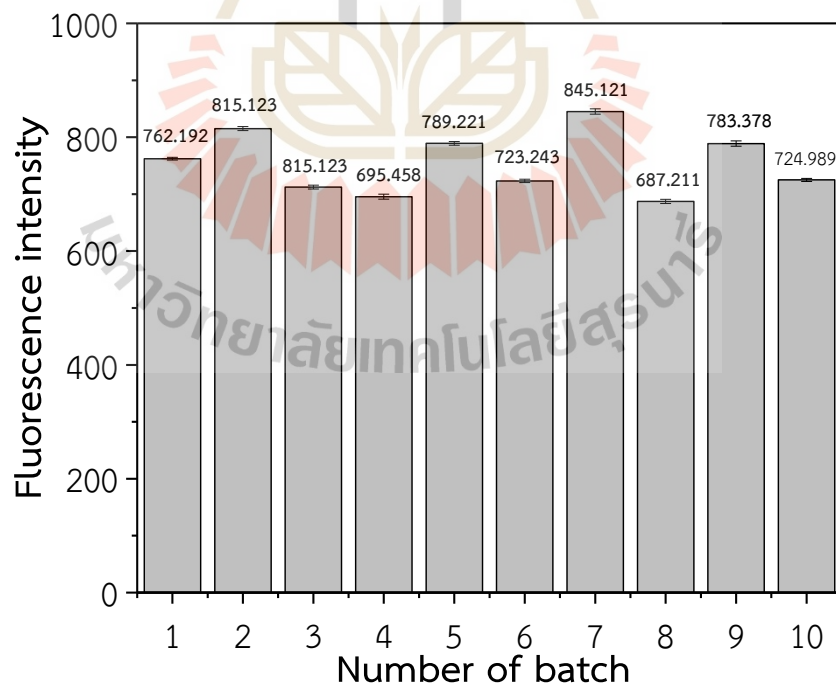


Figure 4.24 Fluorescence signals of sensing films at 506 nm, (a) films from the same batch, (b) films from different batches.

4.7 Performance characteristics of sensing films

4.7.1 Response of sensing film to paraquat

The pyranine-MSF was investigated as a sensing film for the detection of PQ by immersing it into a 10 mL buffer solution for 10 minutes and recording the fluorescence signal at 506 nm. The signal was denoted as I_0 . After that, the sensing film was immersed into a 10 mL PQ solution buffer at pH 6.0 for a certain duration, and the fluorescence signal was measured. The measured signal was denoted as I . The results are shown in Figure 4.25. The fluorescence intensity of the sensing film when placed in PQ solution decreased, as shown in Figure 4.25a. The decreased intensity could be from a charge transfer complex formation between pyranine and PQ, with Pyranine acting as an electron donor and PQ as an electron acceptor (Zhao et al., 2018, Borba et al., 2018). When pyranine is photoexcited, the proton dissociates from the hydroxyl group of pyranine, producing a pyranine cation radical and an electron. PQ accepted the electron, forming a photo-inactive complex (Borba et al., 2018).

Figure 4.25b shows time profiles of signal responses to PQ of the sensing films. The relative signal responses of the sensing film approached a plateau in about 10 minutes for PQ solutions ranging from 1-20 ppm (3.89×10^{-6} - 7.78×10^{-5} M). It was observed that at a longer soaking time, pyranine leached slightly into the solution. To minimize the leaching, one method is to make the sensing film more stable in the buffer solution by coating it with a 1% Nafion solution through dip coating and drying it at room temperature. However, when making the measurements in PQ solutions, it took longer for the signals to approach a plateau than those made with the films without Nafion coating, as shown in Figure 4.26. Therefore, to compromise between the leaching and the time for signal measurements, the sensing films without Nafion coating and a measurement time of 5 min were selected for further study.

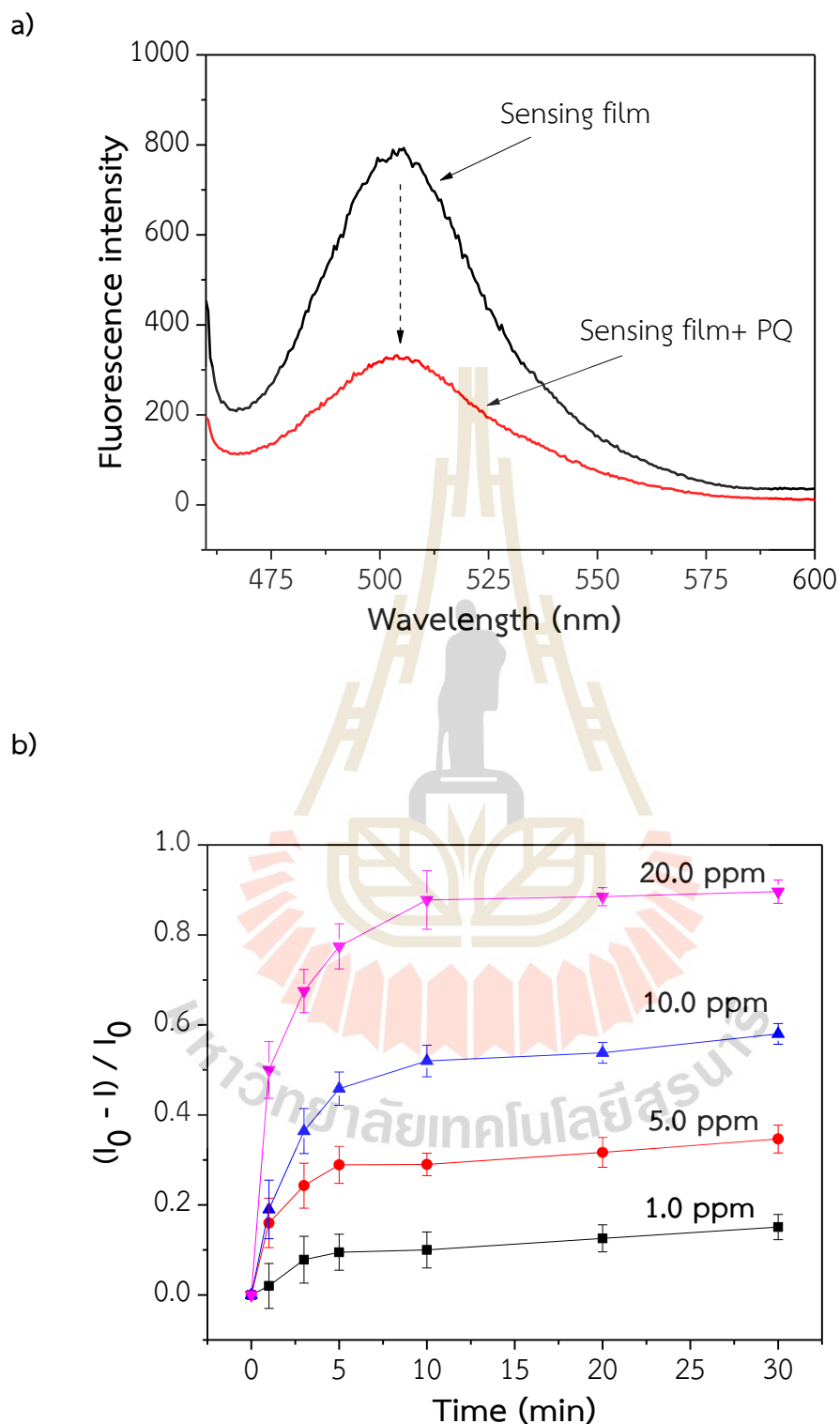


Figure 4.25 a) Fluorescence emission spectra of a sensing film before and after immersing in 10.0 ppm (3.89×10^{-5} M) paraquat solution, b) Time profiles of response signals at 506 nm of the sensing films with paraquat at different concentrations.

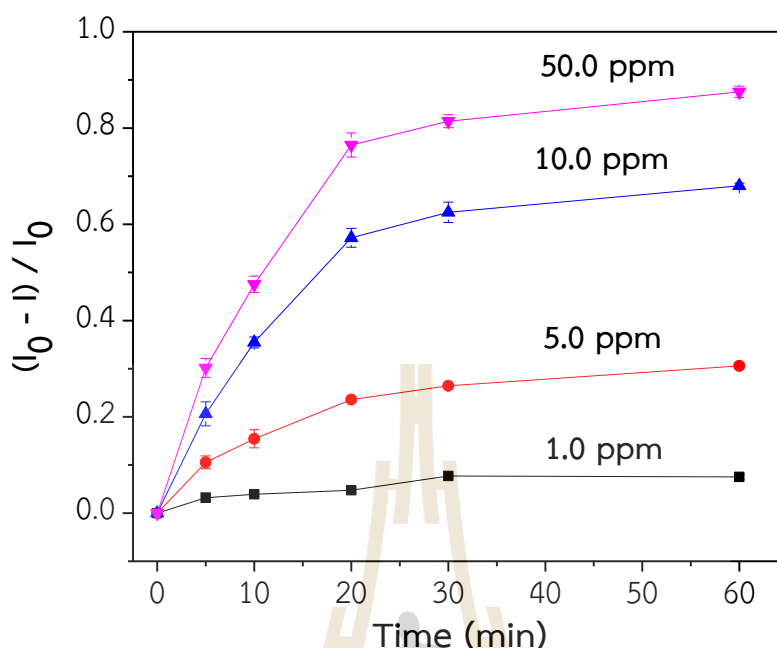


Figure 4.26 Time profiles of response signals of the sensing films coated with Nafion.

4.7.2 Calibration graph for paraquat

The fluorescence quenching of pyranine by paraquat can be expressed mathematically using the Stern-Volmer Equation (4.1) as follows:

$$I_0/I = 1 + K_{SV}[Q] \quad (4.1)$$

The Stern-Volmer Equation utilizes several variables: I_0 is the fluorescence intensity of a sensing film after being immersed in a buffer with a pH of 6.0 for 10 minutes, I is the fluorescence intensity of the film after being submerged in a paraquat solution, K_{SV} is the Stern-Volmer constant, and $[Q]$ represents the concentration of paraquat. $(I_0/I)-1$ was plotted against the paraquat concentration to generate a calibration curve.

The calibration curve for PQ concentration was obtained using a solution volume of 10 mL and a response time of 5 minutes. The results are shown in Figure 4.27. A linear graph with a concentration range of 1-10 ppm was obtained. The linear correlation equation is $y = 0.0793x + 0.0091$, with a coefficient (R^2) 0.9927. The limit of detection (LOD) was calculated to be 0.80 ppm using Equation (4.2):

$$\text{LOD} = 3 \times \text{SD}_{bk} / m \quad (4.2)$$

where SD_{bk} is the standard deviation of the blank measurements and m is the slope of the calibration curve.

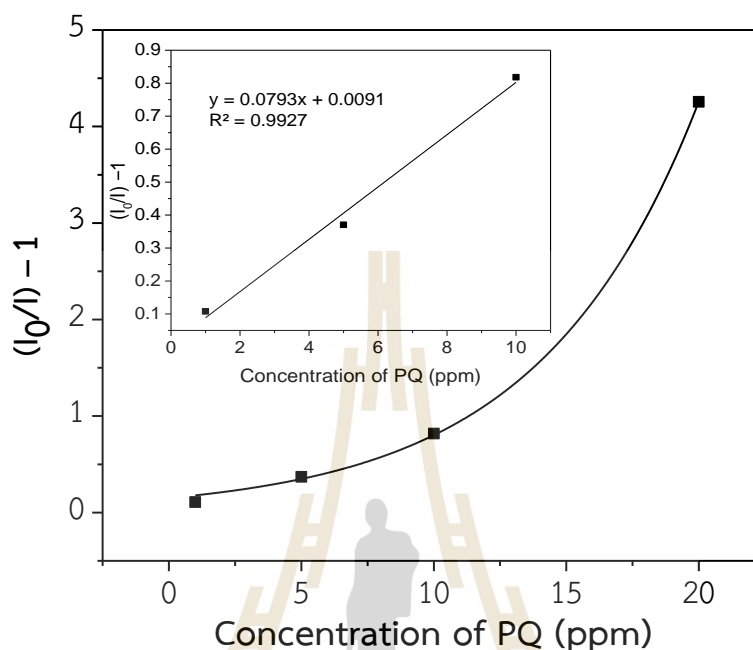


Figure 4.27 Calibration curve for paraquat. An inset shows a linear relationship for PQ concentration range of 1-10 ppm.

4.7.3 Reproducibility and regeneration

The reproducibility of the sensing films' responses to PQ was evaluated by monitoring the fluorescence signals of five sensing films in a 5.0 ppm PQ solution at 506 nm for 5 minutes. The results indicated that the films responded to PQ in a highly reproducible manner, with the RSD of 4.4%. Furthermore, three sensing films were evaluated for their responses in a series of PQ solutions at the concentrations of 3.0, 5.0, and 10.0 ppm. The results, shown in Figure 4.28, indicated that the signals from each film at the same PQ concentration were similar. The RSDs were 0.9%, 3.7%, and 3.0% for 3.0 ppm, 5.0 ppm, and 10.0 ppm PQ solutions, respectively.

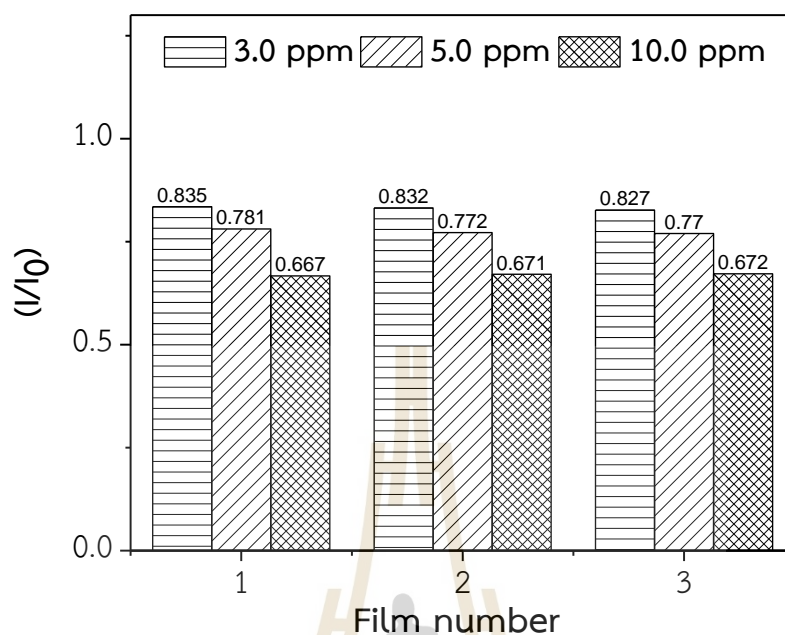


Figure 4.28 The recycling process for one sensing film.

The regeneration of a sensing film was investigated. After the film was exposed to a 10.0 ppm PQ solution, the sensing film was placed in a 0.01 M phosphate buffer pH 7.0 to remove PQ. Figure 4.29 illustrates that the initial signal of the film slightly decreased after the first regeneration, and a similar pattern was observed in subsequent regeneration cycles. The I/I_0 ratios of the first three replicate measurements using the same sensing film showed the RSD of 5.3%. However, the RSD increased to 7.8% for four replicate measurements, indicating that the film could be reused up to three times for consistent results. The decrease in initial fluorescence intensity could be due to incomplete PQ removal from the sensing film and the leaching of pyranine, which could affect its stability and limit its repetitive use.

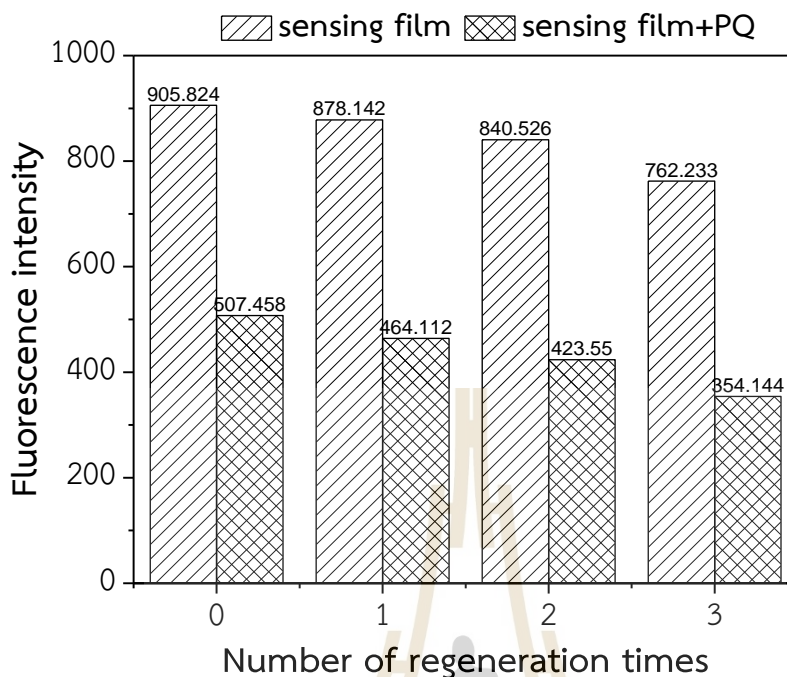


Figure 4.29 Regeneration of the sensing film.

4.7.4 Interference study

The effect of foreign species, Cu^{2+} , Fe^{2+} , Zn^{2+} , K^+ , and carbaryl, on the response of the sensing films to PQ was investigated. These species were selected based on their ability to complex with pyranine and their possible presence in the samples from which the samplings were made. Fluorescence signal measurements of the sensing films were taken in PQ solutions both with and without the tested species. The molar ratio of PQ to the tested species was 1:5, with a fixed PQ concentration of 3.90×10^{-5} M. The changes in the fluorescence signal of the sensing film in the presence of the tested species were expressed as %error calculated according to Equation (4.3). Table 4.1 summarizes the findings, showing that none of the tested species significantly changed the sensor response to PQ, as the error was less than 1.4%.

$$\% \text{Error} = 100 \times (I_{r, \text{PQ/tested species}} - I_{r, \text{PQ}}) / I_{r, \text{PQ}} \quad (4.3)$$

where I_r is the quenching fraction defined as $(I_0 - I) / I_0$, $I_{r, \text{PQ/tested species}}$ is the quenching fraction of the film in a PQ solution in the presence of the tested species, and $I_{r, \text{PQ}}$ is the quenching fraction of the film in a PQ solution without the tested species.

Table 4.1 Interference study at 1:5 molar ratio of PQ to tested species.

Tested species	% Error*
Cu ²⁺	1.08
Fe ²⁺	0.53
Zn ²⁺	1.34
K ⁺	0.31
Carbaryl	0.55

4.8 Real sample analysis

The effectiveness of the developed sensor was demonstrated by measuring PQ in real samples. PQ was not detected in the measured sugarcane peel or tap water samples. A PQ standard solution was incorporated into the real samples to obtain 10 ppm PQ sample solutions for further analysis of the samples. The resulting data is presented in Table 4.2. The retrieved recoveries and RSDs confirm the dependability of the developed technique for PQ measurements in both water and sugarcane peel samples.

Table 4.2 Determination of PQ in tap water and sugarcane peel samples.

Sample	Spiked (ppm)	Found (ppm) ^a	%Recovery	%RSD
Tap water	0	ND ^b	-	-
Tap water	10.0	9.90±0.16	99.0	1.6
Sugarcane peel	0	ND ^b	-	-
Sugarcane peel	10.0	10.10±0.51	101.0	5.1

^a The reported values were the average ± standard deviation (n = 3). ^b ND = not detected

Table 4.3 compares the developed method in this study to other optical methods. The present work has a linear range and detection limit for PQ among the those reported in the literature. Additionally, immobilizing the sensing reagent on a solid support provides a simple means of manipulating the sensor and enables the possibility of recycling the material.

Table 4.3 Different methods used for the detection of PQ.

Sensor material	Detection technique	Linear range (μM)	Limit of detection (μM)
Imidacloprid stabilized silver nanoparticles ^a	Colorimetry	20–180	6.3
Gold nanoparticles modified with 3-mercaptopropanesulfonate ^b	Colorimetry	0.004–1.9	0.004
Citrate coated AgNPs ^c	Colorimetry	0.2–194	0.19
Nitrogen doped graphene quantum dots/Hg ²⁺ ^d	Fluorescence	0.2–7.8	0.074
CdSe/ZnS quantum dots ^e	Fluorescence (quenching)	3.8×10^{-5} –0.2	0.012
Squaraine ^f	Fluorescence Colorimetry	0–140	0.372
Ascorbic acid in basic medium ^g	(multisyringe flow injection analysis)	0.02–1.0	0.003
Pyr-APTES-MSF (this work)	Fluorescence (quenching)	3.9–39	3.5

^{a, b, c, d, e, f, g} Ali et al., 2022, Zhang et al., 2020, Siangproh et al., 2017, Du et al., 2019, Duran et al., 2013, Tu et al., 2015, Maya et al., 2011, respectively.

CHAPTER V

CONCLUSIONS

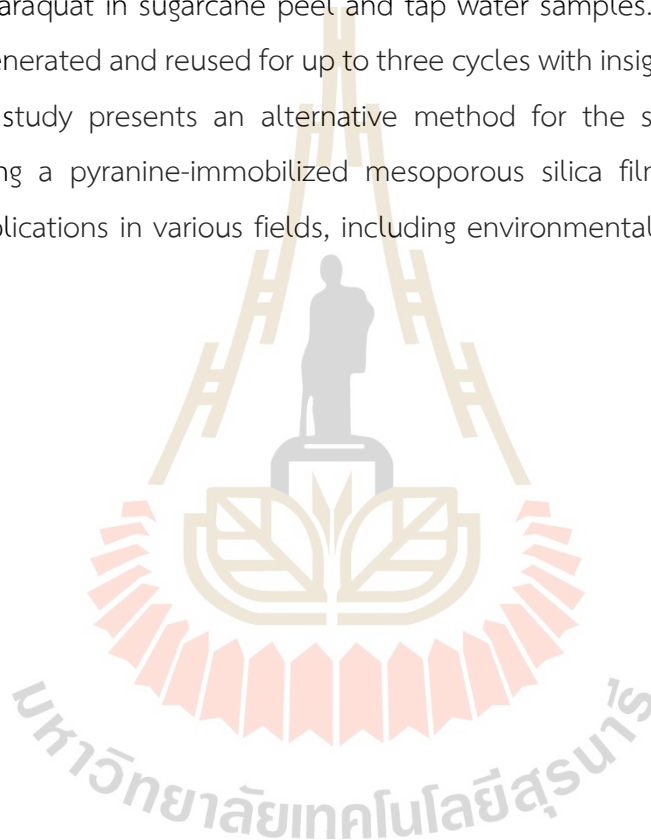
The detection of paraquat is of great importance due to its high toxicity and potential health hazards. In this study, we report on an optical chemical sensor that pyranine was immobilized onto mesoporous silica films modified with aminopropyl groups for the selective detection of paraquat. An electrochemically assisted self-assembly method was employed to deposit mesoporous silica film onto fluorine-doped tin oxide glass. Before pyranine immobilization, the mesoporous silica film was modified with varying concentrations of 3-aminopropyl triethoxysilane. The immobilization of pyranine was achieved through electrostatic interactions between the negatively charged pyranine molecule and the positively charged amino groups on the mesoporous silica surface.

Sodium silicate and tetraethyl orthosilicate were used as silica sources to synthesize mesoporous silica film. Tetraethyl orthosilicate was preferred over sodium silicate due to the better properties of the obtained film, including homogeneity, optical transparency, and film continuity on the substrate. Single- and multiple-layered films were also fabricated and immobilized with pyranine. The single-layered mesoporous film was better suited for pyranine immobilization as the fabricated sensing films appeared more homogeneous.

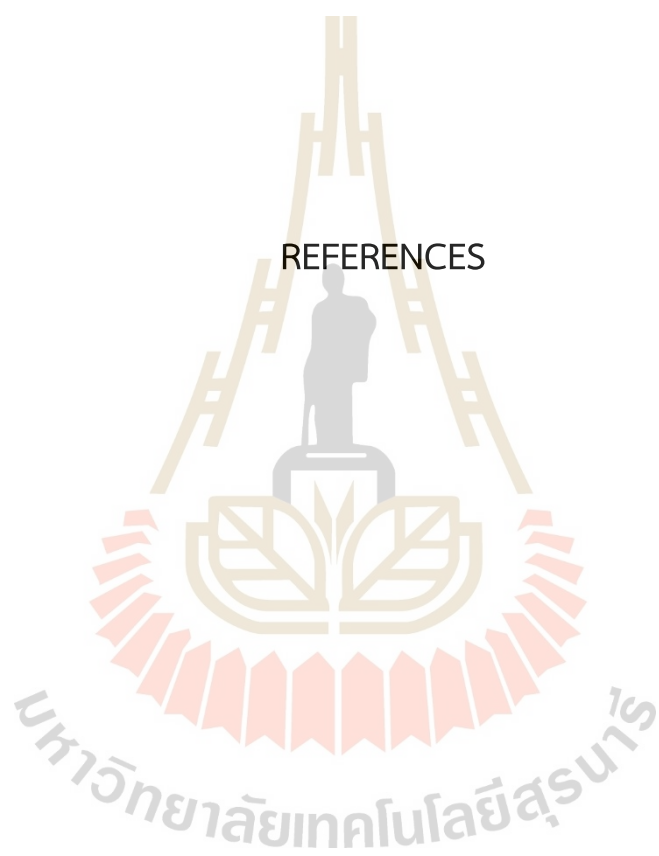
Several techniques were used to characterize the films, including cyclic voltammetry, scanning electron microscopy, transmission electron microscopy, Fourier transform infrared spectroscopy, and fluorescence spectroscopy. Pyranine-immobilized films fluoresced at 506 nm with an excitation at 450 nm, and the fluorescence signal was reduced in the presence of paraquat. The detection

mechanism was attributed to the interaction between paraquat and pyranine, which resulted in the quenching of the fluorescence signal of pyranine. Films modified with 3% 3-aminopropyl triethoxysilane were optimized for paraquat detection. Under the optimum measurement condition, the pH of solutions was fixed at 6.0 and the signal was taken at 5 minutes after the sensing film was exposed to a paraquat solution.

The developed method provided a linear response to paraquat in the 1 to 10 ppm concentration range with a detection limit of 0.80 ppm. The method was applied to quantify paraquat in sugarcane peel and tap water samples. The developed films could be regenerated and reused for up to three cycles with insignificant loss of signals. Overall, this study presents an alternative method for the selective detection of paraquat using a pyranine-immobilized mesoporous silica film, which could have potential applications in various fields, including environmental monitoring and food safety.



REFERENCES



REFERENCES

- Ali, S., Shah, M.R., Hussain, S., Khan, S., Latif, A., Ahmad, M., and Ali, M. (2022). A facile approach based on functionalized silver nanoparticles as a chemosensor for the detection of paraquat. *Journal of Cluster Science*. 33, 413-420.
- Baldini, F., Chester, A. N., Homala, J., and Martellucci, S. (2006). Optical Chemical Sensors. (pp. 77-98). Netherlands: Springer.
- Borba, E.B.de, Amaral, C.L.C., Politi, M.J., Villalobos, R., Baptista, M.S. (2000). Photophysical and photochemical properties of pyranine/methyl viologen complexes in solution and supramolecular aggregates a switchable complex. *Langmuir*. 16, 5900–5907.
- Bus, J.S., Aust, S.D., and Gibson, J.E. (1976). Paraquat toxicity: proposed mechanism of action involving lipid peroxidation. *Environmental Health Perspectives*. 16, 139-146.
- Cheng, J., Rathi, S.J., stradins, P., Frey, G.L., collins, R.T., and Williams, K.R. (2014). Free standing silica thin films with highly ordered perpendicular nanopores. *RSC Advances*. 4, 7627-7633.
- Dansby-Sparks, R.N., Jin, J., Mechery, S.J., Sampathkumaran, U., Owen, T.W., Yu, B.D., Goswami, K., Hong, K., Grant, J., and Xue, Z.L. (2010). Fluorescent-dye-doped sol-gel sensor for highly sensitive carbon dioxide gas detection below atmospheric concentration. *Analytical Chemistry*. 82, 593-600.
- Ding, L., and Su, B. (2015). An electrochemistry assisted approach for fast, low-cost and gram-scale synthesis of mesoporous silica nanoparticles. *RSC Advances*. 5, 65922-65926.
- Ding, L., Li, W., Sun, Q., He, Y., and Su, B. (2014). Gold nanoparticles confined in vertically aligned silica nanochannels and their electrocatalytic activity toward ascorbic acid. *Chemistry-A European Journal*. 20, 12777-12780.

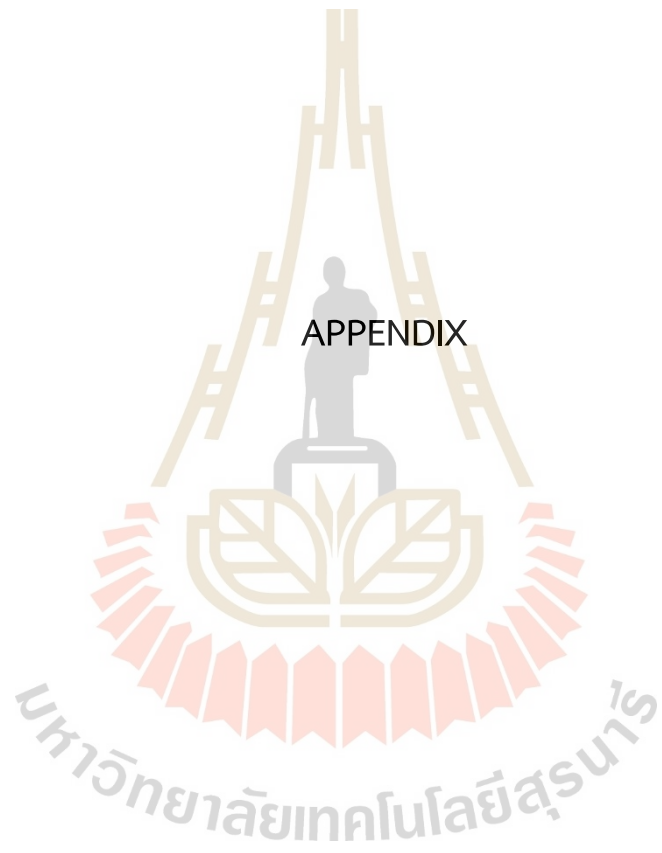
- Du, F., Sun, L., Zen, Q., Tan, W., Chaen, Z., Ruan, G., and Li, J. (2019). A highly sensitive and selective “on-off-on” fluorescent sensor based on nitrogen doped graphene quantum dots for the detection of Hg^{2+} and paraquat. *Sensors and Actuators, B: Chemical*. 288, 96-103.
- Duràn, G.M., Contento, A.M., and Ríos, Á. (2013). Use of Cdse/ZnS quantum dots for sensitive detection and quantification of paraquat in water samples. *Analytica Chimica Acta*. 801, 84-90.
- Etienne, M., Goux, A., Sibottier, E., and Walcarius, A. (2009). Oriented mesoporous organosilica films on electrode: a new class of nanomaterials for sensing. *Journal of Nanoscience and Nanotechnology*. 9, 2398-2406.
- Farook, A., Kasim, H.M., and Hasnah, O. (2010). Synthesis of mesoporous silica immobilized with 3-[(mercapto or amino)propyl]trialkoxysilane by a simple one-pot reaction. *Chinese Journal of Chemistry*. 28, 2383-2388.
- Gao, L., Liu, J., Yuan, H., and Deng, X. (2015). Solid-phase microextraction combined with GC-MS for determination of diquat and paraquat residues in water. *Chromatographia*. 78, 123-130.
- Giordano, G., Vilà, N., Aubert, A., Ghanbaja, J., and Walcarius, A. (2017). Multi-layer, vertically-aligned and functionalized mesoporous silica film generated by sequential electrochemically assisted self-assembly. *Electrochimica Acta*. 237, 227-236.
- Goux, A., Etienne, M., Aubert, E., Lecomte, C., Ghanbaja, J., and Walcarius, A. (2009). Oriented mesoporous silica films obtained by electro-assisted self-assembly (EASA). *Chemistry of Materials*. 21(4), 731-741.
- Grosso, D., Cagnol, F., Soler-Illia, G.J.A.A., Crepaldi, E.L., Amenitsch, H., Brunet-Bruneau, A., Bourgeois, A., and Sanchez, C. (2004). Fundamentals of mesostructuring through evaporation-induced self-assembly. *Advanced Functional Materials*. 14, 309-322.
- Hakonen, A., and Hulth, S. (2008). A high-precision ratiometric fluorosensor for pH: Implementing time-dependent non-linear calibration protocols for drift compensation. *Analytica Chimica Acta*. 606, 63-71.
- Han, J., and Burgess, K. (2010). Fluorescent indicators for intracellular pH. *Chemical Reviews*. 110, 2709-2728.

- Innocenzi, P., and Malfatti, L. (2013). Mesoporous thin films: properties and applications. *Chemical Society Reviews*. 42, 4198-4216.
- Kanno, Y., Suzuki, T., Yamauchi, Y., and Kuroda, K. (2012). Preparation of Au nanowire films by electrodeposition using mesopores silica films as a template: vital effect of vertically oriented mesopores on substrate. *Journal of Physical Chemistry*. 116, 24672-24680.
- Kolberg, D.I.S., Mack, D., Anastassiades, M. Hetmanski, M.T., Fussell, R.J., Meijer, T., and Mol, H.G.J. (2012). Development and independent laboratory validation of a simple method for the determination of paraquat and diquat in potato, cereals and pulses. *Analytical and Bioanalytical Chemistry*. 404, 2465-2474.
- Lu, J., Fan, Y., Howard, M.D., Vaughan, J.C., and Zhang, B. (2017). Single-molecule electrochemistry on a porous silica-coated electrode. *Journal of the American Chemical Society*. 139, 2964-2971.
- Majoul, N., Aouida, S., and Bessaïs, B. (2015). Progress of porous silicon APTES-functionalization by FTIR investigations. *Applied Surface Science*. 331, 388-391.
- Maya, F., Estels, J.M., Cerdà, V. (2011). Improved spectrophotometric determination of paraquat in drinking waters exploiting a multisyringe liquid core waveguide system. *Talanta*. 85, 588-595.
- Nasir, T., Herzog, G., Hébrant, M., Despas, C., Lui, L., and Walcarius, A. (2018). Mesoporous silica thin film for improved electrochemical detection of paraquat. *ACS Sensors*. 3, 484-493.
- Nasir, T., Vodolazkaya, N.A., Herzog, G., and Walcarius, A. (2019). Critical effect of film thickness on preconcentration electroanalysis with oriented mesoporous silica modified electrodes. *Electroanalysis*. 31, 202-207.
- Nivens, D.A., Schiza, M.V., and Angel, S.M. (2002). Multilayer sol-gel membranes for optical sensing applications: Single layer pH and dual layer CO₂ and NH₃ sensors. *Talanta*. 58, 543-550.
- Peter, B., Wartena, M., Kampinga, H.H., and Konings, A.W. (1992). Role of lipid peroxidation and DNA damage in paraquat toxicity and the interaction of paraquat with ionizing radiation. *Biochemical Pharmacology*. 43, 705-715.

- Pizzutti, T.R., Vela, G.M.E., Kok, A. Scholten, J.M., Dias, J.V., Cardoso, C.D., Concenço, G., and Vivian, R. (2016). Determination of paraquat and diquat: LC-MS method optimization and validation. *Food Chemistry*. 209, 248-255.
- Saha, T., Sengupta, A., Hazra, P., and Talukdar, P. (2014). In vitro sensing of Cu^+ through a green fluorescence rise of pyranine. *Photochemical & Photobiological Sciences*. 13, 1427-1433.
- Sha, O., Wang, Y., Chen, X. B., Chen, J., and Chen, L. (2018). Determination of paraquat in environmental water by ionic liquid-based liquid phase extraction with direct injection for HPLC. *Journal of Analytical Chemistry*. 73(9), 862-868.
- Shah, M.T., Alveroglu, E., and Balouch, A. (2018). Pyranine functionalized Fe_3O_4 nanoparticles for the sensitive fluorescence detection of Cu^{2+} ions. *Journal of Alloys and Compounds*. 767, 151-162.
- Siangproh, W., Somboonsuk, T., Chailapakul, O., and Songsrirote, K. (2017). Novel colorimetric assay for paraquat detection on-silica bead using negatively charged silver nanoparticles. *Talanta*. 174, 448-453.
- Stöber, W., and Fink, A. (1968). Controlled growth of monodisperse silica spheres in the micron size range. *Journal of Colloid and Interface Science*. 26, 62-69.
- Suwannaboot, N., Jangkakul, N., Thamjariyawat, Y. Nimcharoen, C., Keawkumay, C., Osakoo, N., Wittayakun, J. (2022). Extraction of silica from sugarcane leaves for synthesis of zeolite as ethylene adsorbent to preserve fresh fruit. *Suranaree Journal of Science and Technology*. 30(2), 1-6.
- Tcheumi, H.L., Tassontio, V.N., Tonle, I.K., and Ngameni, E. (2019). Surface functionalization of smectite-type clay by facile polymerization of β -cyclodextrin using citric acid cross linker: application as sensing material for the electrochemical determination of paraquat. *Applied Clay Science*. 173, 97-106.
- Teng, Z., Zheng, G., Dou, Y., Li, W., Mou, C., Ghanbaja, J., and Walcarius, A. (2012). Highly ordered mesoporous silica films with perpendicular mesochannels by a simple stöber -solution growth approach. *Angewandte Chemie International Edition*. 51, 2173-2177.
- Tomková, H., Sokolová, R., Opletal, T., Kučerová, P., Kučera, L. Součková, J., Skopalová, J., and Barták, P. (2018). Electrochemical sensor based on phospholipid modified

- glassy carbon electrode-determination of paraquat. *Journal of Electroanalytical Chemistry*. 821, 33-39.
- Tsai, W.T. (2013). A review on environmental exposure and health risks of herbicide paraquat. *Toxicological and Environmental Chemistry*. 95(2), 197-206.
- Tu, J., Xiao, L., Jiang, Y., He, Q., Sun, S., and Xu, Y. (2015). Near-infrared fluorescent turn-on detection of paraquat using an assembly of squaraine and surfactants. *Sensors and Actuators, B: Chemical*. 215, 382-387.
- Ulrich, S., Osypova, A., Panzarasa, G., Rossi, R.M., Bruns, N., and Boesel, L.F. (2019). Pyranine-modified amphiphilic polymer conetworks as fluorescent ratiometric pH sensors. *Macromolecular Rapid Communications*. 40, 1900360.
- Walcarius, A., Sibottier, E., Etienne, M., and Ghanbaja, J. (2007). Electrochemically assisted self-assembly of mesoporous silica thin films. *Nature Materials*. 6, 602-608.
- Yao, F., Liu, H., Wang, G., Du, L., Yin, X., and Fu, Y. (2013). Determination of paraquat in water samples using a sensitive fluorescent probe titration method. *Journal of Environmental Sciences*. 25(6), 1245-1251.
- Zhang, Y., Huang, Y., Fu, L., Qiu, J., Wang, Z., and Wu, A. (2020). Colorimetric detection of paraquat in aqueous and fruit juice samples based on functionalized gold nanoparticles. *Journal of Food Composition and Analysis*. 92, 103574.
- Zhao, Z., Zhang, F., and Zhang, Z. (2018). A facile fluorescence "turn-off" method for sensing paraquat based on pyranine-paraquat interaction. *Spectrochimica Acta Part A: Molecular and Biomolecular Spectroscopy*. 199, 96-101.

APPENDIX



APPENDIX

REDOX PROBES FOR MSF CHARACTERIZATION

Ruthenium hexaamine ion, $\text{Ru}(\text{NH}_3)_6^{3+}$, is a cationic probe used for mesoporous film characterization by cyclic voltammetry. This complex is known for its reversible redox couple behavior and its ability to move through the hexagonal mesoporous channels to interact with the electrode substrate. A half-reaction involving the probe species is shown in equation (A1).



Iron hexacyanoferrate, $\text{Fe}(\text{CN})_6^{3-}$ is an anionic probe to investigate the permeability of mesoporous silica film. Like ruthenium hexaamine ion, this complex exhibits reversible redox couple behavior as shown in equation (A2) and moves through the positively charge-modified hexagonal mesoporous channels to interact with the electrode substrate.



CURRICULUM VITAE

SUDARAT SOMBATSRI

Education

- 2002 B.Sc. in Chemistry, Ubon Ratchatane University, Thailand
- 2008 M.Sc. in Chemistry, Suranaree University of Technology, Thailand
- 2023 Ph.D. candidate in Chemistry, Suranaree University of Technology,
Thailand

Experience

- 2003-2004 Chemist, QA. Section, C-Tech Consultant Co, Ltd, Thailand.
- 2004-2006 Chemist, QC. Section, Olan-Kemed Co, Ltd, Thailand.
- 2009-2011 Lecturer, Roi Et Rajabhat University, Thailand.
- 2013-Present Lecturer, Rajamangala University of Technology Isan, Thailand.

Scholarship

- 2017-2022 Rajamangala University of Technology Isan for a Ph.D. scholarship.

Publication

- Sombatsri, S., Deekamwong, K., Khemthong, P., and Prayoonpokarach, S. (2023).
Pyranine immobilized aminopropyl-modified mesoporous silica film for paraquat
detection. *Chemosensors*. 11, 249.